Incorporation of energy-consumption optimization into multi-objective and robust port multi-equipment integrated scheduling

Lei Cai[a,b,c], Wenfeng Li[a,b,*], Huanhuan Li[c], Bo Zhou[d], Lijun He[a,b], Wenjing Guo[a,b], Zaili Yang[c,*]

[a] *State Key Laboratory of Maritime Technology and Safety, Wuhan University of Technology, Wuhan 430063, P. R. China*

[b] *School of Transportation and Logistics Engineering, Wuhan University of Technology, Wuhan 430063, P. R. China*

[c] *Liverpool Logistics, Offshore and Marine Research Institute, Liverpool John Moores University, Liverpool L3 3AF, UK*

[d] *School of Computer Science and Mathematics, Liverpool John Moores University, Liverpool John Moores University, L3 3AF, UK*

Abstract: Port operational efficiency and energy consumption are pivotal, but sometimes contradictory factors influencing its competitiveness. In light of this, the simultaneous optimization of these two objectives within the port integrated scheduling of quay cranes, internal vehicles, and yard cranes, can aid in sustaining port development in the era of digitalization and autonomy. Furthermore, given the persistent fluctuations in uncertain operation time of the cranes and vehicles in port, it becomes imperative to consider the robustness of their scheduling plans collectively. This paper therefore aims to develop a new tri-objective mixed-integer programming model for the first time that enables the incorporation of operational uncertainty and energy efficiency into the context of port operation scheduling consideration. The three objectives are makespan, energy consumption, and scheduling plan robustness, which is represented by anti-cascade and robustness evaluation indices. To effectively address complex optimization challenges, a novel multi-objective solution algorithm has been developed, featured with a dynamic fitness evaluation method selection mechanism. This mechanism utilizes a new crowding distance operator based on the cosine distance of objective value vectors to enhance population diversity in the early stages of the algorithm's iterations. At the later stages, it employs a fuzzy correlation entropy operator to ensure rapid convergence and high-quality solutions. Comparative experiments conducted in scenarios involving emerging technologies such as U-shaped ports and double-cycling operational mode demonstrate the evident improvements achieved by the new model in terms of makespan, energy consumption, and computational efficiency. Based on the compelling experimental results, meaningful insights and implications are put forward, including the potential time and energy savings in port operations, and the practical applicability of these models and algorithms in both port and various other industries.

Keywords: Port integrated scheduling; Anti-cascade and robustness evaluation index; Fuzzy correlation entropy; Energy-efficient; Double-cycling operation

1. Introduction

Shipping plays a fundamental role in sustaining global trade, carrying roughly 80% of the total trade volumes worldwide (Li and Yang, 2023). Ports serve as indispensable logistics nodes connecting land and sea and ensure the success of shipping (Guo et al., 2021). Because of the bottleneck effect, ports need to achieve a high level of operational efficiency to maintain their competitiveness (He et al., 2019). However, in the context of the worldwide commitment towards achieving carbon neutrality, port enterprises have to

* Corresponding authors.
E-mail addresses: liwf@whut.edu.cn (Wenfeng Li), Z.Yang@ljmu.ac.uk (Zaili Yang)

make efforts to reduce carbon emissions and energy consumption (Iris and Lam, 2019; Venturini et al., 2017; Xin et al., 2015, 2014). Further, the juxtaposition of optimizing operational efficiency and energy preservation sometimes creates a paradox (Iris and Lam, 2019; Tan et al., 2021). Improving operational efficiency, which frequently involves increased operational speed of port equipment, often requires higher energy consumption. Therefore, some ports have begun implementing emerging port layouts and operational modes to achieve both energy and operational efficiency (Iris and Lam, 2019; Zhen et al., 2018).

An emerging port layout, referred to as the U-shaped layout (see Fig. 1), has found its successful application in *Qinzhou, Guangxi,* China. Different from traditional layouts, the U-shaped port design enables (Interval Vehicles) IVs to better access deeper sections of the yard and hence effectively improve its operational efficiency. This design enables IVs to travel longer distances and reduce the movement of YCs, thereby decreasing the energy consumption of the heavier YCs (He et al., 2015; Niu et al., 2022). Further, the U-shaped port segregates External Vehicles (EVs) from IVs. Thereby, the adoption of more efficient and energy-saving IVs, such as Intelligent Guided Vehicles (IGVs) leveraging advanced unmanned driving technology, becomes more feasible. The U-shaped layout combines the advantages inherent in traditional port layouts, improving operational efficiency by approximately 30% and reducing energy consumption by approximately 20%, as officially reported by the *Guangxi* provincial government (Guangxi Government, China, 2022). A double-cycling operation mode (Ahmed et al., 2021; Zhang et al., 2015) is evident to be an effective approach to improving the operational efficiency in ports. As illustrated in Fig. 1, in this mode, after an IV completes the transportation of an imported container from the shoreside to the yard, it can then transport an exported container from the yard to the shoreside. The advantage of this operation mode is its ability to reduce unnecessary no-load travel of the IVs, ultimately enhancing the port's operational and energy efficiency (Lee et al., 2015; Zhu et al., 2022).

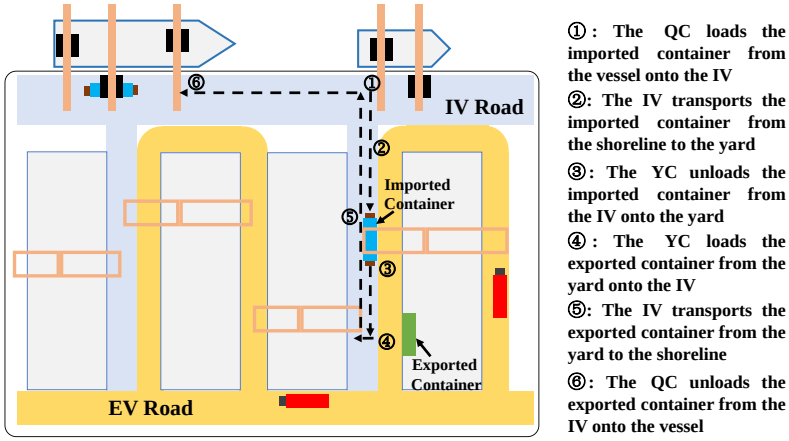

Fig. 1. U-shaped port layout and a simple example of an IV's double-cycling operation.

Given the introduction of advanced port layout and operational mode, new scheduling and efficient coordination of the port's operational equipment become essential to achieve optimization of both energy and operational efficiency. Among the port operational equipment, Quay Cranes (QCs), Yard Cranes (YCs), and IVs emerge as pivotal components. They are responsible for handling imported containers from vessels to the yard and facilitating exported container handling from the yard to vessels. Cai et al. (2024) conducted integrated scheduling experiments of these three types of equipment on a U-shaped port layout, employing a double-cycling operation mode. However, they solely focused on optimizing operational efficiency and failed to address energy efficiency, which made the developed algorithm's applicability in practice questionable, given today's growing concern about decarbonization in the port industry. Consequently, there is a need to develop new scheduling models and algorithms that enhance the port's operational efficiency while

simultaneously reducing energy consumption.

Moreover, uncertainty such as sudden equipment failures is a common factor influencing port operations and can significantly affect a scheduling plan and hence render the optimization of pre-scheduling ineffective (He et al., 2019; L. Li et al., 2023; Li et al., 2024; Liu et al., 2022; Xiang et al., 2018; Zhen et al., 2022). While the advancement of automation, digitization, and intelligence in equipment has reduced such uncertainty through improved monitoring and maintenance measures, uncertainty can only be controlled to a certain level and cannot be eliminated entirely. For instance, it is often the case that an equipment's actual operation time shows a slight difference from the planned due to various factors such as weather conditions and/or driver behavior (Tan and He, 2021). It is even worse if and when minor fluctuations occur on each of the involved equipment generating a collective cascade effect to significantly affect the reliable execution (see Fig.2) (Cai et al., 2023a, 2024). This phenomenon will lead to a reduction in the optimization performance of the scheduling plan, particularly in terms of *makespan* and energy consumption. To assess the ability of a scheduling plan to anti-cascade effect, Cai et al. (2023a) initially proposed an Anti-cascade Effect and Robustness Evaluation Index (AEREI) of the plan.

The AEREI concentrated on the time intervals between operations on the Gantt chart of the scheduling plan (see the green line in Fig. 2) and argued that when confronted with similar *makespans*, the scheduling plan featuring more numerous and uniformly distributed time intervals exhibits greater resilience. These time intervals can be viewed as buffers capable of absorbing operation time fluctuations to a certain degree. The time intervals adjacent to operations with a higher degree of uncertainty will also be assigned higher weights. It is evident that when two schedules have a similar *makespan*, the schedule with the higher index is considered superior. Given the index's excellent performance and fitness in previous research (Cai et al., 2023a, 2024), this paper continues to integrate it into the optimization objective. This integration can enhance the robustness of the scheduling plan, thereby maintaining its optimization performance in terms of both operational and energy efficiency.

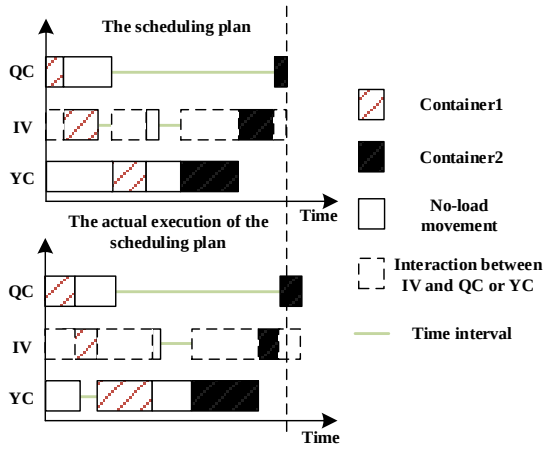

Fig. 2. The uncertainty of operation times and the time intervals of the scheduling.

To summarize, the primary questions this paper addresses are the following. **Research Question 1** is: In the emerging context of U-shaped port layouts and double-cycling operation modes, how can to formulate a scheduling plan for QCs, IVs, and YCs that can simultaneously achieve both operational and energy efficiency, while also ensuring the plan's robustness? The solution lies in incorporating *makespan*, *energy consumption*, and the AEREI as the multiple optimization objectives in the development of an integrated scheduling plan for these three types of equipment. This approach effectively transforms the original problem into a tri-objective optimization challenge.

In this tri-objective integrated scheduling problem involving QCs, IVs, and YCs within ports, it's evident

that the robustness of the pre-scheduling plan may be contradictory to the objective of minimizing the *makespan*. In such scenarios, the application of a multi-objective optimization method based on the Pareto Frontier (PF), such as NSGA-II (Non-Dominated Sorting Genetic Algorithm II) emerges as the most suitable approach. However, one of the difficulties of employing multi-objective optimization based on PF is how to devise an effective strategy for evaluating the fitness of the population solutions by synthesizing the three objectives to enhance convergence efficiency. Another challenge is how to select the most appropriate population solution among the numerous solutions within the PF while excluding subjective human factors. The third challenge is that the traditional crowding distance operator in NSGA-II is over simplistic and fails to effectively maintain population diversity.

Hence, **Research Question 2** emerges: How can we develop an efficient multi-objective optimization algorithm that produces a suitable scheduling plan to optimize three objectives within an acceptable computation time? This question can be addressed by implementing novel fitness evaluation mechanisms based on the cosine distance of objective value vectors and Fuzzy Correlation Entropy (FCE) theory. The idea behind the developed algorithm is that, at the beginning of the iteration, the algorithm primarily uses the fitness evaluation operator based on objective cosine distance to improve population diversity. In the later stages of the iteration, the FCE operator is more likely to be employed to facilitate quick convergence and help select the most suitable solutions.

In NSGA-II, the fitness evaluation method relies solely on traditional crowding distance. While this method effectively evaluates population diversity, it has exposed a disadvantage in terms of calculating crowding distance within each Pareto rank without reflecting the true diversity of the entire population. To address this, a novel fitness evaluation operator is designed for solutions' crowding distance that compares the cosine distance of solutions' objective value vectors within the population, providing an appropriate evaluation of population diversity for the first time. To decrease computational complexity, the cosine distances of each solution's objective value vector with the objective value vectors of the ideal points are compared. This allows for the sorting of the distances. Subsequently, it is only necessary to compare the cosine distances of adjacent solutions' objective value vectors. This method streamlines the computation while maintaining accurate diversity evaluation. Furthermore, the fitness evaluation mechanism based on FCE theory has undergone pilot testing in practice by studies conducted by He et al. (2022) and Li et al. (2022). This mechanism eliminates the dependency of the algorithm on objective weights and significantly reduces computational time. Under this mechanism, each population solution is assigned a ρ value known as the fuzzy correlation entropy coefficient. With the help of this coefficient, decision-makers can effortlessly identify the population solution with the highest coefficient as the final solution. This paper pioneers the feasibility study of using these two solution fitness evaluation operators in the realm of port scheduling by developing a novel multi-objective optimization algorithm, thereby ensuring a harmonious balance between solution diversity and rapid convergence.

In conclusion, this paper tackles two crucial research questions (i.e., **Q1**-**Q2**), providing corresponding solutions (i.e., **S1**-**S2**) for each:

Q1: How can effective schedules for QCs, IVs, and YCs be developed to concurrently optimize operational and energy efficiency, as well as ensure the robustness of these scheduling plans in an emerging U-shaped port layout and double-cycling operation mode?

S1: It is recommended to implement a tri-objective integrated scheduling of QCs, IVs, and YCs that involves optimizing *makespan*, energy consumption, and the anti-cascade effect and robustness evaluation index, simultaneously.

Q2: How can a proficient multi-objective optimization algorithm be developed to generate an appropriate

scheduling plan that optimizes three objectives within an acceptable computational timeframe?

S2: It is suggested to develop a novel multi-objective optimization algorithm that incorporates a dynamic fitness evaluation method selection mechanism. This mechanism integrates fitness evaluation methods based on the cosine distance of objective value vectors and the FCE coefficient.

The subsequent organization of this paper is outlined as follows. Section 2 describes a systematic literature review through which the state-of-the-art study field is defined, existing research gaps are identified, and the contributions of this study are presented. In Section 3, the research problem is expounded upon, along with the presentation of a tri-objective integrated scheduling model. Section 4 provides an in-depth discussion of the methodology, with a particular focus on the tri-objective optimization algorithm. Section 5 encapsulates the presentation and discussion of the experimental results as well as the research findings and implications. Section 6 concludes the research findings and research limitations and offers insights into prospects.

2. Systematic literature review

This section begins with an overview of the research status of port resources integrated allocation and scheduling. Subsequently, it narrows its focus to the integrated scheduling of QCs, IVs, and YCs concerning uncertainty, and conducts a critical analysis.

2.1. General review

2.1.1. Procedure

A general literature review was conducted to gain a comprehensive overview of port resources integrated allocation and scheduling. The Web of Science (WoS) core collection database was used to retrieve peer-reviewed journal papers from 1985 to 2023, resulting in 578 papers. After carefully reviewing the titles, keywords, and abstracts, 112 journal papers were selected for further analysis. The port resources considered in this review include equipment resources such as QCs, YCs, vehicles, and further, human resources, space resources like berth and yard, and other resources such as energy. Notably, vessel resources, such as vessel stowage, were not considered a part of the port resources and were excluded from the scope of this study.
The distribution of the papers over the years, as well as the number of papers for each type of integrated allocation and scheduling problem and their published journals, were counted and analyzed. The *VOSviewer* tool was employed for network visualization and overlay visualization of the co-occurrence map of terms found in the titles, keywords, and abstracts of the selected papers. For a detailed illustration of the procedure, please refer to Fig. 3. The detailed explanation of the new findings from Fig.3 is given in the ensuing sections.

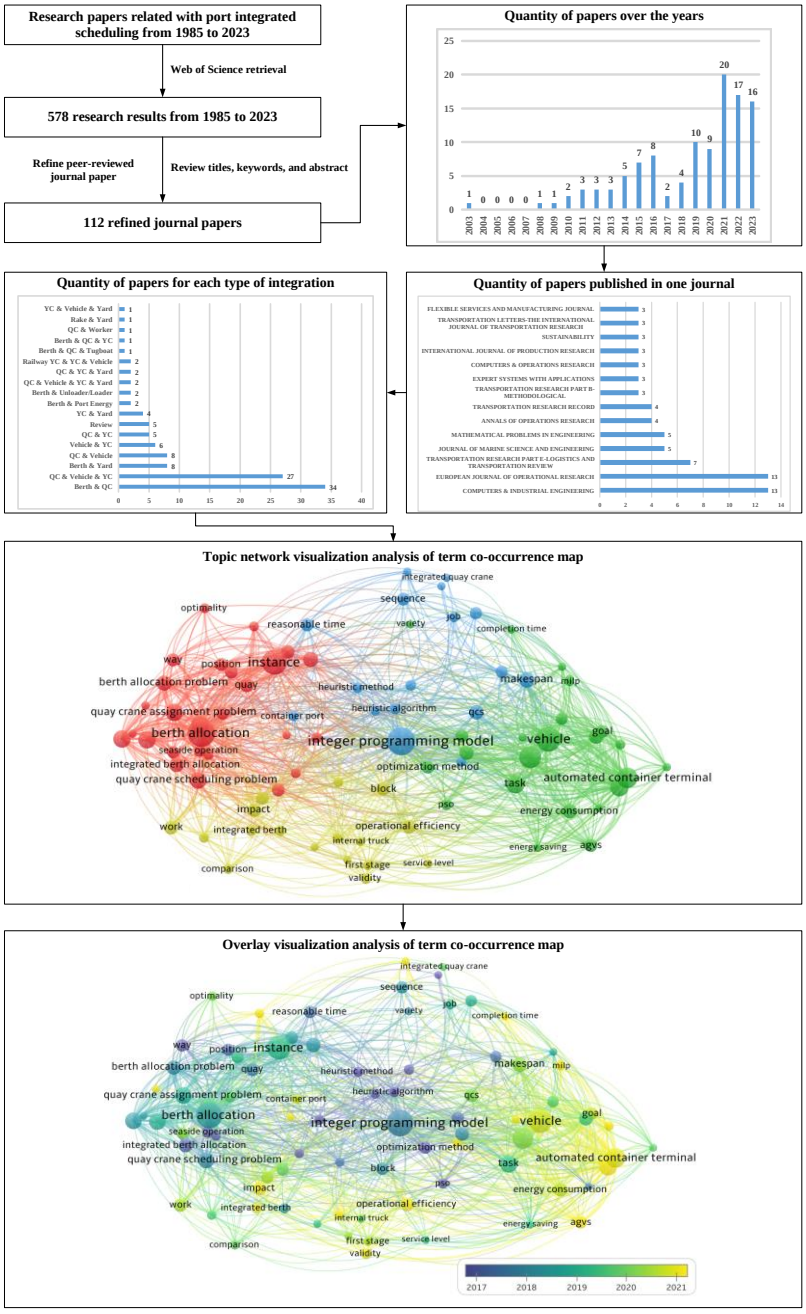

Fig. 3. The procedure of the general literature review.

2.1.2. Current research status

In terms of the number of papers published over the years, it is evident that research on port resources integrated allocation and scheduling has shown a steady upward trend (Chen et al., 2020). The total number of associated papers indicates that this research topic remains a hotspot and continues to garner significant attention.

Regarding the quantity of papers for each type of integrated problems, the most focused area is the berth and QCs integrated assignment or scheduling problem. This is because vessel berthing times have a high correlation with QCs' handling time, making it a crucial aspect to consider (Chargui et al., 2021; Guo et al., 2022; Yu et al., 2023). Additionally, the integrated scheduling problem of QCs, vehicles, and YCs is the second most emphasized area. These three equipment types represent three essential stages that a container undergoes (Yue et al., 2023), and this scenario can be treated as a three-stage hybrid flow shop scheduling

problem. The simultaneous consideration of these three equipment types makes the research focus innovative.

From the perspective of the number of papers published in specific journals, journals related to industrial engineering, operation research, and transportation have published the most papers on this topic. Journals such as *Computers & Industrial Engineering, European Journal of Operational Research*, *Transportation Research Part E-Logistics and Transportation Review*, among others, have been at the forefront of disseminating research in this area.

2.1.3. In-depth analysis

The minimum occurrence of a term is set as 4, considering only the presence or absence of a term in a document, without taking into account the number of occurrences in a document. The research topic network visualization figure reveals four distinct clusters, each corresponding to a specific topic. Analyzing the high-frequency co-occurrence terms in each cluster helps decipher the meaning of each topic. The four clusters represent the following topics:

1) The integrated scheduling problem related to berths, shown in red, includes keywords such as *berth allocation, instance*, *vessel*, q*uay crane scheduling problem*, *quay crane assignment*, etc.

2) The integrated scheduling problem related to vehicles, shown in green, includes keywords like *vehicle*, *automated container terminal*, *energy consumption, AGVs*, etc.

3) The mathematical models and relevant solution algorithms, displayed in blue, encompass keywords such as *integer programming model*, *makespan*, *bi-level genetic algorithm*, *heuristic algorithm*, *heuristic method*, etc.

4) The experimental performance, depicted in yellow, involves keywords like *comparison*, *validity*, *operational efficiency*, *experimental results*, *cplex*, etc. These topics encompass both practical problems and solution methods related to port resources integrated allocation and scheduling.

Several new insightful findings are drawn from the network visualization. 1) The berth allocation problem is closely linked with the quay crane assignment or scheduling problem, aligning with the previous analysis of the number of papers for each type of integration. 2) The most mentioned optimization objective in the existing literature is *makespan*, followed by *energy consumption*. *Makespan* is a crucial factor for port operational efficiency and is commonly considered in most scheduling problems. On the other hand, *energy consumption* is associated with port energy efficiency, aligning with the trend of green ports and industry. 3) *Energy consumption* is often connected with vehicles, indicating a focus on optimizing the energy consumption of vehicles due to the deployment of electric unmanned IVs like AGVs (Automated Guided Vehicles) and IGVs (Intelligent Guided Vehicles) in ports. However, it is essential to note that the energy consumption of cranes should be further optimized as cranes consume more energy than vehicles when they travel the same distance, especially in U-shaped ports where this phenomenon is more pronounced. 4) The mathematical models developed in the literature are typically mixed-integer programming models, and heuristic algorithms are most commonly used. This is because, in actual port operations, scheduling plans need to be generated within limited computation time. Accurate solution algorithms become impractical when dealing with large-scale problems. Hence, heuristic algorithms are favored for their efficiency and practicality.

The overlay visualization figure reveals several research trends over the years, including 1) The integrated problem associated with berth allocation has reached a relatively mature stage and has been the subject of research for many years. 2) The integrated scheduling problem involving vehicles has been gaining momentum in recent years, indicating that it has become a research hotspot. 3) *Makespan* remains a traditional optimization objective, but the optimization of *energy consumption* has garnered much attention in recent years due to the global development strategy of promoting low-carbon and environmental protection. 4) The use of mixed-integer programming models and heuristic algorithms has been prevalent for many years

and is considered a traditional approach in the field.

Upon comprehensive analysis of the two figures, the research gaps in the field become evident: 1) The absence of co-occurrence terms related to "*uncertainty*" or "*robustness*" suggests that these aspects have not been well addressed over the years. Nevertheless, neglecting uncertainty implies that the scheduling plan is more likely to lack practicality in the real port operational environment. Therefore, addressing uncertainty and incorporating robustness into scheduling solutions have to be explored further. 2) The lack of co-occurrence terms such as "*multi-objective*" indicates that the majority of existing research has focused on single-objective optimization. In the current era, focusing solely on the optimization of a single objective, such as *makespan*, falls short of meeting the fast-growing demands in practice. More research on multi-objective optimization, particularly concerning *energy consumption*, is needed with urgency given the climate change concerns and the UN's sustainability development goals. 3) Co-occurrence terms representing new characteristics of port layout or operational modes, such as "*double-cycling*" and "*U-shaped*," are yet reflected in the current state-of-the-art studies, despite their increasing use in the real world. Nonetheless, as port operations advance, these emerging technologies are gaining prominence, enhancing port efficiency and underscoring the necessity for in-depth research to explore their novel characteristics.

2.2. Refined review

Following a general review of research pertaining to port resources integrated allocation and scheduling, eight papers specifically addressing the integrated scheduling of QCs, IVs, and YCs with a focus on uncertainty are meticulously selected. These papers will be analyzed in-depth focusing on the following key aspects: optimization objectives, types of uncertainty, port operation modes and layouts, the methods employed, case studies, and problem scales. This analysis is organized into subsections 2.2.1, 2.2.2, and 2.2.3, respectively. Table 1 presents a comparison between this paper and the eight papers discussed, based on the aforementioned aspects.

Table 1. Literature review on integrated scheduling of QCs, IVs, and YCs under uncertainties.

Paper	Optimization objective	Types of uncertainty				Is the double-cycling mode considered?	Port layout	Method
		Uncertain operation time			General disturbance			
		QC	YC	IV				
Zeng and Yang, 2009	*Makespan*	√	√			×	?	MIP−>GA(DR+NN)−>DES
Homayouni et al., 2014	*Total traveling time of equipment, delays in cranes tasks*	√	√			×	?	GA
Lu and Le, 2014	*Completion time of YCs*		√	√		×	Traditional parallel layout	MIP−>PSO(MCS)
Zeng et al., 2015	*Operation times of QCs, reshuffling times of exported*	√	√			√	?	MIP−>GA−> DES

Tang et al., 2020	*containers Balance of energy consumption*				√	√	?	MAS−>DR
Ahmed et al., 2021	*Productivity rate*, *Vessel turn-around time*, *Total cost*	√	√	√		√	?	DES
Cahyono et al., 2022	*Makespan*				√	×	Traditional perpendicular layout	DES(HA)
Cai et al., 2023	*Makespan*	√	√	√		×	?	MIP−>GA(AEREI)
Cai et al., 2024	*Makespan*, *Robustness*	√	√	√		√	U-shaped port	Bi-objective MIP(AEREI)−>NSGA-II
This study	*Makespan*, *Energy consumption*, *Robustness*	√	√	√		√	U-shaped port	Tri-objective MIP(AEREI)−>FEM(FCE)

Notes: AEREI: Anti-cascade Effect and Robustness Evaluation Index; DES: Discrete Event Simulation; DR: Dispatching Rule; FCE: Fuzzy Correlation Entropy; FEM: Fitness Evaluation Mechanism; GA: Genetic Algorithm; HA: Heuristic Algorithm; MAS: Multi-Agent Simulation; MCS: Monte Carlo Simulation; MIP: Mixed-Integer Programming; NN: Neural Network; NSGA-II: Non-Dominated Sorting Genetic Algorithm II; PSO: Particle Swarm Optimization; (): Inclusion or Priority Relation; √: True; ×: False; +: Coordinate Relation; −>: Progressive Relation; ?: Unknown

Several new insights can be gleaned from Table 1: 1) There is a conspicuous lack of research associated with port integrated scheduling that simultaneously optimizes *makespan* and *energy consumption*, let alone enhances the robustness of the scheduling plan. 2) Given the regularity of the uncertain operation time addressed in this paper, a proactive scheduling approach is the most suitable methodology to devise a robust scheduling plan. 3) The emerging U-shaped port layout and double-cycling operation, epitomizing high operational and energy efficiency, have not yet received adequate attention within the port integrated scheduling problem. 4) While many studies focus on small or medium-scale scenarios, there is a significant gap in research addressing large-scale situations, such as the scheduling of 2,000 containers.

Furthermore, from the general review mentioned above, four papers on port scheduling that discuss the robustness assessment indicator have been meticulously selected for further analysis. This selection aims to validate the rationality of the anti-cascade effect and robustness evaluation index used in this paper. The detailed analysis is presented in Subsection 2.2.4.

2.2.1. Optimization objectives and types of uncertainty

The majority of the existing related studies address single-objective optimization problems, with *time*-related objectives such as *makespan* being prevalent. This prominence is due to the fact that *time*-related objectives reflect the operational efficiency of the port and significantly impact its profitability.

In a review paper on energy efficiency in ports by Iris and Lam (2019), it was noted that with the growing emphasis on low-carbon and environmental protection initiatives, researchers have begun to pay attention to

energy consumption-related objectives. However, they also highlighted that integrated port resource scheduling, particularly those related to *energy* awareness, offers a promising perspective that deserves further attention. In terms of relevant research, while Tang et al. (2020) focused primarily on achieving a balance in *energy consumption* among different equipment, they did not optimize their total energy consumption. Consequently, there is considerable scope for further exploration in this field, particularly in the comprehensive consideration of both *makespan* and *energy consumption* aspects.

In terms of the types of uncertainty, *time*-related uncertainty is the most addressed in the current literature. The majority of studies have directed their attention towards the uncertain operation time of cranes or vehicles. Notably, two studies, namely Tang et al. (2020) and Cahyono et al. (2022), have touched upon the broader concept of general disturbance. In this context, general disturbance denotes situations where the exact nature of the uncertainty is not explicitly specified. The preference for *time*-related uncertainty can be attributed to the fact that other uncertainties, such as *equipment failure*, occur less frequently due to regular equipment maintenance and repairs. Consequently, given the ubiquity and complexities associated with uncertain operation times in port scheduling, it emerges as the most prominently studied form of uncertainty.

In essence, within the existing literature on integrated scheduling of port three-stage equipment, there is a notable absence of studies that concurrently optimize *makespan*, *energy consumption*, and scheduling plan *robustness* – a new motivation for this study.

2.2.2. Methods employed

One approach to handling uncertainty is the proactive scheduling approach (Rodrigues and Agra, 2022). The proactive scheduling approach aims to create a robust pre-scheduling plan by analyzing the characteristics or predictions of uncertainty. Once executed, the plan is capable of absorbing or withstanding uncertainty to a certain extent. Lu and Le (2014) employed the Monte Carlo Simulation (MCS) method, which incorporated parameters associated with uncertainty, to compute the fitness function of the Particle Swarm Optimization (PSO) algorithm while considering uncertain operation time. Cai et al. (2023a, 2024) conducted an analysis of the cascading effects resulting from uncertain operation time fluctuations. They devised an AEREI to assess the pre-scheduling plan's robustness.

Another strategy to tackle uncertainty is the reactive scheduling approach, which can be categorized into predictive-reactive and completely-reactive scheduling approaches. In the predictive-reactive approach, an initial pre-scheduling plan is formulated, which is then adjusted or regenerated in response to uncertain events (Xiang et al., 2018). In contrast, the completely-reactive scheduling approach fails to develop a comprehensive scheduling plan and often allocates scheduling tasks locally based on specific dispatching rules or simulation logic (Cai et al., 2023b, 2022).

Among the existing studies, the predictive-reactive scheduling approach has not yet been applied in the field with success, possibly due to its more fitting application in handling emergencies. There appears to be no associated research thus far that specifically addresses emergencies. The completely-reactive scheduling approach does not establish a comprehensive global pre-scheduling plan. Consequently, this approach is better suited for managing real-time disruptions and handling general disturbances. In line with the completely-reactive scheduling approach, Tang et al. (2020) employed the *AnyLogic* simulation software to construct a Multi-Agent Simulation (MAS) model representing the operational processes of QCs, IVs, and YCs. Ahmed et al. (2021) integrated uncertainty into two simulation models to compare the double-cycling mode and the single-cycling mode. Cahyono et al. (2022) developed a Discrete Event Simulation (DES) model that integrates the operations of QCs, IVs, and YCs, and the allocation of storage positions for containers in both the yard and vessels. They introduced a Heuristic Algorithm (HA) named model predictive algorithm into the DES model to aid in obtaining a near-optimal solution.

Furthermore, Zeng and Yang (2009) utilized the Dispatching Rule (DR) to promptly generate an initial feasible solution, enhancing the quality of GA populations. They devised a surrogate model based on a Neural Network (NN) to predict the objective value of GA. In their research, uncertainty in crane operation time was present in their DES. They incorporated uncertain parameters into the DES to simulate a more realistic experimental environment, rather than directly addressing uncertainty. Homayouni et al. (2014) conducted a sensitivity analysis to examine the impacts of uncertain operation times of cranes on the integrated scheduling method. Notably, they did not directly address the issue of uncertainty. Zeng et al. (2015) assumed a uniform distribution for the processing time of cranes and utilized it as input parameters in the GA. Although concerning uncertainty, these studies have yet to actively address it comprehensively.

In the selected papers, some focused on analyzing the impact of uncertainty on integrated scheduling while the others used the completely-reactive scheduling approach or the proactive scheduling approach to deal with the uncertainty, depending on the nature of the uncertainty being tackled. In the scenarios involving general disturbances lacking clear patterns, the completely-reactive approach is more applicable. On the other hand, when dealing with uncertain operation times that exhibit a level of regularity, the proactive scheduling approach becomes better. Considering the problem's characteristics, this paper employs a proactive scheduling approach to generate robust scheduling plans.

2.2.3. Port operation modes, layouts, case studies

In tandem with the evolution of intelligent ports striving for heightened efficiency, the operational modes and layouts of ports have undergone significant transformations over time. For instance, Homayouni et al. (2014) delved into a novel equipment type known as Split-Platform Automated Storage/Retrieval System (SP-AS/RS), which can be considered akin to a YC or an automated stereoscopic warehouse. Zeng et al. (2015) and Tang et al. (2020) explored the double-cycling operational mode of QCs. Additionally, Ahmed et al. (2021) investigated the double-cycling operation of QCs, IVs, and YCs, yet only Zeng et al. (2015) among them pursued global optimization.

Within this spectrum of associated research considering uncertainty, the exploration of U-shaped ports—an emergent port layout—and the global optimization considering the double-cycling operation of IVs have remained limited. Only Cai et al. (2024) sought to bridge these notable research gaps, however, they did not consider the optimization of energy consumption.

When considering case studies and problem scales, it becomes evident that the majority of associated studies were grounded in real-world port scenarios. Nonetheless, nearly all of these studies, excluding Ahmed et al. (2021), primarily focused on small or medium-scale problems, with container counts staying below 500. Notably, Ahmed et al. (2021) ventured into a large-scale problem involving 32,000 containers. However, it is worth highlighting that their focus wasn't solely centered on global optimization. Instead, they employed a DES framework to compare the double-cycling and single-cycling operational modes. Capitalizing on the non-iterative nature of DES, results were obtained within a constrained computational timeframe. In alignment with the prevailing practice of real-case studies embraced by the majority of associated research, this study continues in the same vein. Moreover, to enhance practicality, experiments in this study were conducted on a larger scale, encompassing a maximum of 2,000 containers.

2.2.4. Robustness assessment in port scheduling

Robustness assessment has become a significant area of interest in recent years, and research in this field remains growing. This assessment quantifies the robustness of schedules under uncertain conditions, addressing an ability that typical stochastic programming and robust optimization methods do not provide. As detailed in the recent literature review by Li et al., (2024) on port scheduling in uncertain environments, four primary approaches to assessing robustness have been identified: 1) The AEREI, which is utilized in this

manuscript; 2) The incorporation of buffer or slack time, referred to as time intervals in our methodology, within the scheduling plans, as explored by Dik and Kozan, (2017) in QC scheduling, and by Wu and Zhu, (2023) in berth allocation and quay crane scheduling; 3) The sensitivity of scheduling plans to uncertainties, exemplified by Homayouni et al. (2014) in their study on integrated scheduling of QCs, IVs, and YCs; 4) The probability of scheduling plan failures or incurring losses due to uncertainties, as detailed in Chargui et al. (2023) for QC scheduling.

The "sum of slack time" approach, which focuses on the aggregate time intervals between operations, has been previously shown to be of limited effectiveness (Cai et al., 2024, 2023a). The theoretical analysis in the previous section concurs, demonstrating that merely concentrating on the sum of time intervals is not enough; the distribution of these intervals is also crucial. The "sensitivity" approach, depends heavily on the accuracy of predictions regarding how uncertainties influence the scheduling plan's execution. This approach's reliance on predictions, necessary to simulate uncertainty effects and calculate sensitivity values, contrasts with our method, which is independent of such predictions and simpler to implement, both in terms of computational complexity and time required. The "likelihood" approach is generally employed to manage significant uncertainties. For instance, the research by Chargui et al. (2023) evaluated the reliability levels of QCs to develop a proactive scheduling plan that minimizes the likelihood of QC failures. However, like the "sensitivity" approach, it often demands extensive historical data or expert estimations, making it challenging to implement (Stockmann et al., 2021). Moreover, both the "sensitivity" and "likelihood" approaches are unsuitable for the tri-objective optimization problem outlined in this manuscript due to their complex procedures and lengthy computation time.

Table 2 below summarizes the existing robustness assessment approaches in port scheduling and explains why they were not adopted in this paper.

Table 2. The existing robustness assessment approaches employed in port scheduling.

Category	Characteristic	Advantage	Disadvantage	Reasons for choosing or not choosing this approach	Representative reference
Anti-cascade effect and robustness evaluation index	Accumulation, distribution, and importance degree of slack time	Easy to implement; Highly effective, Less knowledge	Ineffective under conditions of large uncertainty, such as equipment failure	Suitable for this tri-objective optimization scenario; Good effectiveness	This paper
Accumulation of slack time	Accumulation of slack time	Easy to implement	Poor effectiveness	Poor effectiveness	Dik and Kozan, (2017); Wu and Zhu, (2023)
Sensitivity of the schedule to uncertainties	Measuring the effects of uncertainties in a simulated environment	Suitable for extensive scenarios; Highly effective when sufficient prior knowledge	Difficult to implement; Extensive computation time and prior knowledge	Unsuitable for this tri-objective optimization scenario; Lack enough prior	Homayouni et al. (2014)

		is available		knowledge	
Likelihood of schedule failures or loss	The likelihood that a schedule's performance will worsen beyond a specified threshold when facing uncertainties	Suitable for extensive scenarios; Highly effective when sufficient prior knowledge is available	Difficult to implement; Extensive computation time and prior knowledge	Unsuitable for this tri-objective optimization scenario, Lack enough prior knowledge	Chargui et al. (2023)

2.3. Research gaps and our contributions

Drawing from the existing research, this paper identifies and outlines four distinct research gaps (i.e., **G1-G3**), which are addressed through four corresponding contributions (i.e., **N1-N3**) that are made through this study.

G1: Few studies have been conducted to concurrently optimize the three objectives of *makespan*, *energy consumption*, and the *robustness* of a scheduling plant that affect port operation efficiency collectively when addressing the integrated scheduling problem of QCs, IVs, and YCs.

N1: A new solution is proposed for the tri-objective integrated scheduling of QCs, IVs, and YCs, taking into account operational efficiency, energy consumption, and the feasibility of the port's scheduling plan amidst uncertainty.

This paper develops a comprehensive tri-objective mixed-integer programming model incorporating the features of the novel U-shaped port layout and the double-cycling operation mode to effectively address this integrated scheduling challenge. The state-of-the-art AEREI from the latest research has been introduced to represent the optimization objective of *robustness*. Consequently, a tri-objective optimization model is formulated, encompassing the comprehensive optimization of *makespan*, *energy consumption*, and schedule *robustness*. Therefore, this paper reveals a novelty in terms of introducing non-0-1 variables that represent the operation completion time and the no-load movement of equipment. These variables are instrumental in calculating energy consumption and the robustness index. Consequently, the model developed in this paper significantly differs from the existing literature including Cai et al. (2024).

G2: Conventional multi-objective optimization algorithms based on the Pareto theory often encounter challenges in evaluating the solution fitness and selecting the most suitable solution from a PF.

N2: A multi-objective optimization algorithm has been developed, incorporating a dynamic fitness evaluation method selection mechanism that utilizes new crowding distance based on the cosine distance of objective value vectors and FCE.

In addition to establishing the relevant chromosome coding, decoding, crossover, and mutation rules specific to this problem, this paper presents a novel multi-objective optimization algorithm. This developed algorithm integrates a dynamic fitness evaluation method selection mechanism and introduces a novel crowding distance evaluation operator based on the cosine distance of solution objective value vectors. The cosine distance of objective value vectors is predominantly used in the early stages of iterations to preserve solution diversity, while the FCE is utilized in the latter stages to enhance convergence efficiency and facilitate the selection of an optimal solution from the PF. Our algorithm uniquely combines FCE with a crowding distance operator designed to increase population diversity. This marks the first integration of its kind in fitness evaluation for multi-objective optimization.

G3: From an applied research perspective, there are few associated studies offering practical insights on

the benefits of tri-objective integrating scheduling of QCs, IVs, and YC for stakeholders.

N3: The experiments are carried out on a larger scale from actual port cases and yield meaningful insights and implications are put forward for both port and various other industries.

The operational parameters, encompassing factors like operation times, unit energy consumption of equipment, and the port layout, are grounded in real-world scenarios. The experimentation scale involves up to 2000 containers, 3 QCs, 2 YCs, and 72 IVs. The experiment results provide key implications for stakeholders such as port authorities, environmental agencies, manufacturing companies, and warehouse operators, focusing on operational efficiency, energy saving, cost reduction, and so on.

3. Preliminary

This section initiates by introducing the problem, specifying the underlying assumptions, and then proceeds to construct the mathematical programming model.

3.1. Problem description and assumptions

The port features a U-shaped layout and is equipped with several IGVs functioning as IVs. The primary role of these IGVs is to transfer imported containers from the shoreline to the yard and to transport exported containers from the yard back to the shoreline. A crucial point to note is the interaction between IGVs and cranes. Whenever a crane is involved in loading or unloading containers, an IGV must pause at the loading/unloading zone and refrain from movement to ensure safety.

Presently, multiple vessels are berthed and awaiting loading and unloading procedures. Detailed information regarding the loading and unloading tasks of both imported and exported containers is available. Notably, an IGV can operate in a double-cycling mode, wherein after completing the transportation task of an imported container, it promptly transitions to executing the transportation task of an exported container. In a double-cycling pair, the import and export containers transported consecutively by an IGV do not necessarily come from the same vessel.

The QCs are responsible for the loading/unloading tasks in the specific bays on the vessel, while the YCs similarly have designated areas of responsibility within the port yard. Therefore, the assignment of which crane will handle each container is predetermined, ensuring the safe distance between cranes and avoiding collisions between them. What remains to be determined is the operational sequence of the containers for each crane, as well as the assignment of each container to a specific IGV and the corresponding operational sequence of containers for each IGV. Here are some additional assumptions:

(1) The total number of equipment available is fixed, with no other equipment exiting or joining in.

(2) No container handling tasks will be added or removed after the commencement of pre-scheduling.

(3) Each equipment can only handle one container at a time.

(4) Each container can only be handled by one equipment during an operation procedure.

(5) Equipment failures are unlikely to occur due to regular monitoring and maintenance.

(6) Given that each crane has assigned areas of responsibility, there will be no conflicts among them.

(7) The actual operational time of the equipment fluctuates around the historical average values.

3.2. Multi-objective mixed-integer programming model

The multi-objective mixed-integer programming model comprises two sections: symbol definition and formulations.

3.2.1. Symbol definitions

Table 3 displays the sets, indices, parameters, 0-1 variables, and non-0-1 variables found within the model.

Table 3. The definitions of symbols.

Symbol	Definition	Symbol	Definition
Set and indices			

C_I	Collection of imported containers	C_E	Collection of exported containers
C	Collection of containers indexed by i or i'. $C = C_I \cup C_E$	M_Q	Collection of QCs
M_Y	Collection of YCs	M_V	Collection of IGVs
M	Collection of equipment indexed by k. $M = M_Q \cup M_Y \cup M_V$	S	Collection of stages that a container must undergo indexed by j
Parameters			
N_I	Total number of import containers	N_E	Total number of export containers
$d_{ii'jk}$	The distance covered by equipment k while moving from the final loading/unloading position of operation o_{ij} to the initial loading/unloading position of operation $o_{i'j}$	o_{ij}	The jth stage of container i. The first stage (j=1) pertains to the QCs loading/unloading operations between vessels and IGVs. The second stage (j=2) corresponds to the IGVs transporting operation between the shoreline and the yard. The third stage (j=3) refers to the YCs loading/unloading operation between IGVs and yard
$\tilde{v}_k$	The uncertain horizontal movement speed of equipment k	$\tilde{t}_{ij}$	The uncertain operation time of o_{ij}
p_{0Q}, p_{0V}, p_{0Y}	The idle power of QCs, IGVs, and YCs	p_{1Q}, p_{1V}, p_{1Y}	The horizontal movement power of QCs, IGVs, and YCs without any load
p_{2V}	The average horizontal moving power of IGVs with load	p_{3Q}, p_{3Y}	The average power of the trolley of the QC or YC during a container lifting and dropping operation
Q_i	The index of QC responsible for loading/unloading container i	Y_i	The index of YC responsible for loading/unloading container i
L	Large enough positive integer	$\sigma_{1_{ij}}$	The standard deviation of the operation time for operation o_{ij}
$\sigma_{2_{ij}}$	The standard deviation of equipment no-load movement time immediately following operation o_{ij}		
0-1 variables			
x_{ik}	If container i is assigned to equipment k, 1; otherwise 0	$y_{ii'jk}$	If operation o_{ij} is processed immediately before $o_{i'j}$ on equipment k, 1; otherwise 0
$g_{ii'}$	If an import container $i \in C_I$ and an export container $i' \in C_E$ are paired to realize a double-cycling transportation of the IGV, 1; otherwise 0	$z_{1_{ii'}}$, z_{2_k}	Auxiliary variables employed for the linearization of constraints
Non-0-1 variables			
Makespan	The completion time of all containers	$S_{1_{ij}}$	The starting time of operation o_{ij}
$C_{1_{ij}}$	The completion time of operation o_{ij}	$S_{2_{ij}}$	The starting time of the no-load movement immediately following operation o_{ij}
$C_{2_{ij}}$	The completion time of the no-load movement immediately following operation o_{ij}	E	The total energy consumption of all equipment throughout the schedule
E_0	The cumulative energy consumption of all equipment during idle periods	E_1	The cumulative energy consumption of all equipment during moving without load
E_2	The cumulative energy consumption of all IGVs during moving with load	E_3	The cumulative energy consumption of all QCs and YCs during the process of lifting and dropping containers
R	The anti-cascade and robustness of the schedule	S_{ij}	The time interval between operation o_{ij} and $o_{i(j+1)}$ of a container i
S_{ijk}	The time interval between operation	I_{ij}, I_{ijk}	The significance degree of the time

	o_{ij} and its subsequent operation with an equipment k interval
R_{ij}, R_{ijk}	The dispersion degree of the time interval

3.2.2. Formulations

The mathematical model comprises objectives and corresponding constraints.

Objectives

$$f_1 = min\ \ Makespan \tag{1}$$

$$f_2 = min\ \ E \tag{2}$$

$$f_3 = min\ \ (-R) \tag{3}$$

f_1 represents the *makespan*, indicating the total time taken for all operations to be completed, reflecting the operational efficiency of the port. f_2 signifies the cumulative *energy consumption* of QCs, IGVs, and YCs during the scheduling period, highlighting the energy efficiency of the port. f_3 corresponds to the anti-cascade and robustness index, providing insights into the schedule's *robustness*. The value of f_3 is taken as the minimum value of the opposite of *R*, as a higher *R* indicates a more robust schedule.

s.t.

1) Mixed-integer programming model of operational process

① *Makespan* constraint

$$Makespan - C_{1_{ij}} \geq 0, \forall i \in C; j \in \{1,3\} \tag{4}$$

Constraint (4) specifies the completion time of all containers.

② Operational time constraints

$$C_{1_{ij}} - S_{1_{ij}} - \tilde{t}_{ij} = 0, \forall i \in C; j \in S \tag{5}$$

$$C_{1_{ij}} - S_{1_{i(j+1)}} \leq 0, \forall i \in C_I; j \in \{1,2\} \tag{6}$$

$$C_{1_{ij}} - S_{1_{i(j-1)}} \leq 0, \forall i \in C_E; j \in \{2,3\} \tag{7}$$

$$S_{1_{i'j}} - C_{1_{ij}} - \frac{d_{ii'jk}}{\tilde{v}_k} + L\left(3 - y_{ii'jk} - x_{ik} - x_{i'k}\right) \geq 0, \forall i, i' \in C; j \in \{1,3\}; k \in M_Q \cup M_Y \tag{8}$$

$$S_{1_{i'j}} - C_{1_{i(j+1)}} - \frac{d_{ii'jk}}{\tilde{v}_k} + L\left(3 - y_{ii'jk} - x_{ik} - x_{i'k}\right) \geq 0, \forall i' \in C; i \in C_I; j \in \{2\}; k \in M_V \tag{9}$$

$$S_{1_{i'j}} - C_{1_{i(j-1)}} - \frac{d_{ii'jk}}{\tilde{v}_k} + L\left(3 - y_{ii'jk} - x_{ik} - x_{i'k}\right) \geq 0, \forall i' \in C; i \in C_E; j \in \{2\}; k \in M_V \tag{10}$$

Constraint (5) enforces the connection between the starting time and the completion time of the operations. Constraints (6)-(7) guarantee that the starting time of the subsequent operation cannot precede the completion time of the last operation for import containers and export containers, respectively. Constraint (8) specifies that if two containers are assigned to the same crane, the starting time of the latter container's operation within the crane's sequence cannot be earlier than the completion time of the former container's operation plus the crane's no-load movement time. Constraints (9) to (10) define that if two containers are assigned to the same IGV, the starting time of the later container's operation within the IGV's sequence cannot precede the completion time of the former container's subsequent operation plus the IGV's no-load movement time. Given the interaction time between IGVs and cranes, the IGVs must wait until the cranes complete the loading/unloading operations before departing.

③ No-load movement time constraints

$$S_{2_{ij}} - C_{1_{ij}} \geq 0, \forall i \in C; j \in S \tag{11}$$

$$C_{2_{ij}} - S_{2_{ij}} - \frac{d_{ii'jk}}{\tilde{v}_k} + L\left(3 - y_{ii'jk} - x_{ik} - x_{i'k}\right) \geq 0, \forall i, i' \in C; k \in M_Q \ \ and \ \ j \in \{1\}; k \in M_V \ \ and \ \ j \in$$

$\{2\}; k \in M_Y \ \ and \ \ j \in \{3\}$(12)

$C_{2_{ij}} - S_{2_{ij}} - \frac{d_{ii'jk}}{\tilde{v}_k} - L\left(3 - y_{ii'jk} - x_{ik} - x_{i'k}\right) \leq 0, \forall i, i' \in C; k \in M_Q \ \ and \ \ j \in \{1\}; k \in M_V \ \ and \ \ j \in$

$\{2\}; k \in M_Y \ \ and \ \ j \in \{3\}$(13)

$C_{2_{ij}} - S_{1_{i'j}} - L\left(3 - y_{ii'jk} - x_{ik} - x_{i'k}\right) \leq 0, \forall i, i' \in C; k \in M_Q \ \ and \ \ j \in \{1\}; k \in M_V \ \ and \ \ j \in$

$\{2\}; k \in M_Y \ \ and \ \ j \in \{3\}$(14)

Constraint (11) ensures that the starting time of the no-load movement immediately following operation o_{ij} cannot precede the completion time of the operation o_{ij}. Constraints (12) and (13) guarantee the relationship between the starting time and the completion time of the no-load movement immediately following operation o_{ij}. Constraint (14) ensures that the starting time of o_{ij}'s subsequent operation in the equipment cannot be earlier than the completion time of the no-load movement immediately following operation o_{ij}.

④ IGVs' double-cycling operation constraints

$$g_{ii'} - 1 + z_{1_{ii'}} \geq 0, \forall i' \in C_E; i \in C_I \quad (15)$$

$$g_{ii'} + x_{ik} + x_{i'k} - 3 + Lz_{1_{ii'}} \geq 0, \forall i' \in C_E; i \in C_I; k \in M_V \quad (16)$$

$$y_{ii'jk} - 1 + Lz_{1_{ii'}} \geq 0, \forall i' \in C_E; i \in C_I; j \in \{2\}; k \in M_V \quad (17)$$

$$y_{ii'jk} - 1 - Lz_{1_{ii'}} \leq 0, \forall i' \in C_E; i \in C_I; j \in \{2\}; k \in M_V \quad (18)$$

Constraints (15) to (18) are the linearized of the constraints $if \ \ g_{ii'} - 1 = 0, \ then \ \ g_{ii'} + x_{ik} + x_{i'k} - 3 = 0 \ \ and \ \ y_{ii'jk} - 1 = 0, \forall i' \in C_E; i \in C_I; j \in \{2\}; k \in M_V$. They describe the process of a double-cycling operation. The variables $z_{1_{ii'}}$ play a vital role in the linearization process. If $g_{ii'} = 1$, it signifies that the import container *i* and the export container i' can participate in a double-cycling operation. Here, constraint (16) ensures that both the import container *i* and the export container i' must be allocated to the same IGV's sequence of tasks. Constraints (17) and (18) ensure that the IGV initially transports the import container *i* and subsequently the export container i'.

⑤ Tasks sequence constraints

$\sum_{i \in C} \sum_{i' \in C} y_{ii'jk} - \sum_{i \in C} x_{ik} + 1 - L\left(1 - z_{2_k}\right) \leq 0, \forall k \in M_Q \ \ and \ \ j \in \{1\}; k \in M_V \ \ and \ \ j \in \{2\}; k \in$

$M_Y \ \ and \ \ j \in \{3\}$(19)

$\sum_{i \in C} \sum_{i' \in C} y_{ii'jk} - \sum_{i \in C} x_{ik} + 1 + L(1 - z_{2_k}) \geq 0, \forall k \in M_Q \ \ and \ \ j \in \{1\}; k \in M_V \ \ and \ \ j \in \{2\}; k \in$

$M_Y \ \ and \ \ j \in \{3\}$(20)

$\sum_{i \in C} \sum_{i' \in C} y_{ii'jk} - \sum_{i \in C} x_{ik} - Lz_{2_k} \leq 0, \forall k \in M_Q \ \ and \ \ j \in \{1\}; k \in M_V \ \ and \ \ j \in \{2\}; k \in M_Y \ \ and \ \ j \in$

$\{3\}$(21)

$\sum_{i \in C} \sum_{i' \in C} y_{ii'jk} - \sum_{i \in C} x_{ik} + Lz_{2_k} \geq 0, \forall k \in M_Q \ \ and \ \ j \in \{1\}; k \in M_V \ \ and \ \ j \in \{2\}; k \in M_Y \ \ and \ \ j \in$

$\{3\}$(22)

$$\sum_{i \in C} x_{ik} - z_{2_k} \geq 0, \forall k \in M_Q \ \ and \ \ j \in \{1\}; k \in M_V \ \ and \ \ j \in \{2\}; k \in M_Y \ \ and \ \ j \in \{3\} \quad (23)$$

$$\sum_{i \in C} x_{ik} - Lz_{2_k} \leq 0, \forall k \in M_Q \ \ and \ \ j \in \{1\}; k \in M_V \ \ and \ \ j \in \{2\}; k \in M_Y \ \ and \ \ j \in \{3\} \quad (24)$$

$\sum_{i' \in C \cup \{N_I + N_E + 1\} \setminus \{i\}} y_{ii'jk} = \sum_{i' \in C \cup \{0\} \setminus \{i\}} y_{i'ijk} = x_{ik}, \forall i \in C; k \in M_Q \ \ and \ \ j \in \{1\}; k \in M_V \ \ and \ \ j \in$

$\{2\}; k \in M_Y \ \ and \ \ j \in \{3\}$(25)

Constraints (19) to (24) guarantee the relationship between the decision variables x_{ik} and $y_{ii'jk}$. They are the linearized versions of the constraints $\sum_{i \in C} x_{ik} - \sum_{i \in C} \sum_{i' \in C} y_{ii'jk} = \begin{cases} 1, if \ \ \sum_{i \in C} x_{ik} \neq 0 \\ 0, if \ \ \sum_{i \in C} x_{ik} = 0 \end{cases}, \forall k \in$ $M_Q \ \ and \ \ j \in \{1\}; k \in M_V \ \ and \ \ j \in \{2\}; k \in M_Y \ \ and \ \ j \in \{3\}$. To be precise, if there are containers handled by the equipment *k*, the cumulative sum count of $y_{ii'jk}$ for given values of *j* and *k* should equal the total count of containers managed by equipment *k* minus one. Constraint (25) ensures that for each container *i*

handled by equipment k, there must be exactly one predecessor and one successor. The predecessor and the successor can include virtual containers indexed by 0 and $N_I + N_E + 1$. The virtual containers are introduced to streamline the formulation. Constraints (19) and (25) collectively ensure the logical rationality of the task sequence within the same equipment.

⑥ Tasks assignment constraints

$$x_{iQ_i} = 1; \forall i \in C \tag{26}$$

$$x_{iY_i} = 1; \forall i \in C \tag{27}$$

$$\sum_{k \in M_Q} x_{ik} = 1; \forall i \in C \tag{28}$$

$$\sum_{k \in M_V} x_{ik} = 1; \forall i \in C \tag{29}$$

$$\sum_{k \in M_Y} x_{ik} = 1; \forall i \in C \tag{30}$$

Constraints (26) to (30) pertain to the allocation of tasks for containers. Constraints (26) to (27) guarantee that containers are allocated to the designated cranes as per the pre-assigned plan. Constraints (28) to (30) guarantee that each container can be allocated to only one equipment at each stage.

⑦ Container double-cycling pairs constraints

$$\sum_{i' \in C_E} g_{ii'} = 1; \forall i \in C_I \tag{31}$$

$$\sum_{i' \in C_I} g_{i'i} = 1; \forall i \in C_E \tag{32}$$

$$\sum_{i \in C_I} \sum_{i' \in C_E} g_{ii'} = N_I = N_E \tag{33}$$

Constraints (31) to (33) signify that each import container must be paired with an export container, and this pairing can only occur once for each container.

⑧ Variables feasible ranges constraints

$$x_{ik}, y_{ii'jk}, g_{ii'}, z_{1_{ii'}}, z_{2_k} \in \{0,1\}, \forall i, i' \in C; k \in M_Q \ \ and \ \ j \in \{1\}; k \in M_V \ \ and \ \ j \in \{2\}; k \in M_Y \ \ and \ \ j \in \{3\} \tag{34}$$

$$S_{1ij} \geq 0, \forall i \in C; j \in S \tag{35}$$

$$C_{1ij} \geq 0, \forall i \in C; j \in S \tag{36}$$

$$S_{2ij} \geq 0, \forall i \in C; j \in S \tag{37}$$

$$C_{2ij} \geq 0, \forall i \in C; j \in S \tag{38}$$

Constraints (34) to (38) establish the feasible range for the variables.

2) Calculation of the energy consumption

$$E = E_0 + E_1 + E_2 + E_3 \tag{39}$$

$$E_0 = \sum_{i \in C} \sum_{i' \in C} \sum_{k \in M_Q} y_{ii'1k} \cdot (S_{1_{i'1}} - C_{1_{i1}} - C_{2_{i1}} + S_{2_{i1}}) \cdot p_{0Q} + \sum_{i \in C} \sum_{i' \in C} \sum_{k \in M_V} y_{ii'2k} \cdot (S_{1_{i'2}} - C_{1_{i2}} - C_{2_{i2}} + S_{2_{i2}}) \cdot p_{0V} + \sum_{i \in C} \sum_{i' \in C} \sum_{k \in M_Y} y_{ii'3k} \cdot (S_{1_{i'3}} - C_{1_{i3}} - C_{2_{i3}} + S_{2_{i3}}) \cdot p_{0Y} \tag{40}$$

$$E_1 = \sum_{i \in C} (C_{2_{i1}} - S_{2_{i1}}) \cdot p_{1Q} + \sum_{i \in C} (C_{2_{i2}} - S_{2_{i2}}) \cdot p_{1V} + \sum_{i \in C} (C_{2_{i3}} - S_{2_{i3}}) \cdot p_{1Y} \tag{41}$$

$$E_2 = \sum_{i \in C} \tilde{t}_{i2} \cdot p_{2V} \tag{42}$$

$$E_3 = \sum_{i \in C} \tilde{t}_{i1} \cdot p_{3Q} + \sum_{i \in C} \tilde{t}_{i3} \cdot p_{3Y} \tag{43}$$

Eq. (39) indicates that the total energy consumption is composed of equipment idle periods, equipment no-load movement, equipment loading movement, and crane loading/unloading operation. Eqs. (40) through (43) compute the energy consumption by multiplying the operational power of the equipment in various scenarios with the corresponding time spent in each scenario. Among these equations, the time for one equipment idle period can be determined by calculating the cumulative sum of the starting operation time of a subsequent container in the equipment task sequence minus the sum of the completion operation time of the immediately preceding container and the time taken for the equipment no-load movement immediately following the operation of the preceding container.

3) Calculation of the anti-cascade and robustness index for the schedule

$$R = \sum R_{ij} + \sum R_{ijk} \tag{44}$$

$$R_{ij} = \begin{cases} 0, \ if \ \ I_{ij} = 0 \\ -I_{ij} \cdot \ln I_{ij}, \ if \ \ I_{ij} \neq 0 \end{cases}, \forall i \in C; j \in S \quad (45)$$

$$R_{ijk} = \begin{cases} 0, \ if \ \ I_{ijk} = 0 \\ -I_{ijk} \cdot \ln I_{ijk}, \ if \ \ I_{ijk} \neq 0 \end{cases}, \forall i \in C; k \in M_Q \ \ and \ \ j \in \{1\}; k \in M_V \ \ and \ \ j \in \{2\}; k \in M_Y \ \ and \ \ j \in \{3\} \quad (46)$$

$$I_{ij} = \begin{cases} \frac{2}{\sigma_{1_{ij}} + \sigma_{1_{i(j+1)}}} \cdot \frac{S_{ij}}{\sum S_{ij} + \sum S_{ijk}}, if \ \ i \in C_I; j \in \{1,2\} \\ \frac{2}{\sigma_{1_{ij}} + \sigma_{1_{i(j-1)}}} \cdot \frac{S_{ij}}{\sum S_{ij} + \sum S_{ijk}}, if \ \ i \in C_E; j \in \{2,3\} \end{cases} \quad (47)$$

$$I_{ijk} = \frac{2}{\sigma_{2_{ij}} + \sum_{i' \in C} y_{ii'jk} \cdot \sigma_{1_{i'j}}} \cdot \frac{S_{ijk}}{\sum S_{ij} + \sum S_{ijk}}, \forall i \in C; k \in M_Q \ \ and \ \ j \in \{1\}; k \in M_V \ \ and \ \ j \in \{2\}; k \in M_Y \ \ and \ \ j \in \{3\} \quad (48)$$

$$S_{ij} = \begin{cases} S_{1_{i(j+1)}} - C_{1_{ij}}, if \ \ i \in C_I; j \in \{1,2\} \\ S_{1_{i(j-1)}} - C_{1_{ij}}, if \ \ i \in C_E; j \in \{2,3\} \end{cases} \quad (49)$$

$$S_{ijk} = \sum_{i' \in C} y_{ii'jk} \cdot (S_{1_{i'j}} - C_{1_{ij}} - C_{2_{ij}} + S_{2_{ij}}), \forall i \in C; k \in M_Q \ \ and \ \ j \in \{1\}; k \in M_V \ \ and \ \ j \in \{2\}; k \in M_Y \ \ and \ \ j \in \{3\} \quad (50)$$

Eq. (44) defines the anti-cascade and robustness index of the schedule as the cumulative sum of the dispersion degree of time intervals. This dispersion degree is computed using Eqs. (45) and (46), which utilize an entropy-based calculation to assess the significance of each time interval between two consecutive operations, both in equipment and in a container, respectively. The significance degree of a time interval is determined by Eqs. (47) and (48), capturing the relative proportion of that time interval among all time intervals. Eqs. (49) and (50) illustrate the method for calculating the time interval between two consecutive operations within a container or equipment.

It is important to note that in Eqs. (47) and (48), terms like $\frac{2}{\sigma_{1_{ij}} + \sigma_{1_{i(j+1)}}}$ and $\frac{2}{\sigma_{2_{ij}} + \sum_{i' \in C} y_{ii'jk} \cdot \sigma_{1_{i'j}}}$ are utilized as coefficients in front of the proportion representing the size of time intervals. The rationale behind this is that $\sigma_{1_{ij}}$ and $\sigma_{2_{ij}}$ denote the standard deviation of the operation time and the subsequent equipment no-load movement time, respectively, for operation o_{ij}. The larger these time intervals adjacent to the operations and the smaller the standard deviation of the operation time and equipment no-load movement time of these operations, the stronger the ability of these time intervals to resist uncertainty. Consequently, this coefficient is designed based on this concept. By employing this method, time intervals adjacent to operations with a higher degree of uncertainty are assigned higher weights.

4. Methodology

In this section, the newly proposed problem-solving framework is first outlined. Following this, the specifics of the developed multi-objective optimization algorithm are delved into, detailing the encoding, decoding, crossover, and mutation rules that have been meticulously crafted for the chromosomes to address this particular problem. Furthermore, the developed multi-objective optimization algorithm is featured with an innovative dynamic fitness evaluation method selection mechanism. This mechanism incorporates fitness evaluation methods based on the cosine distance of objective value vectors and the FCE coefficient, both of which are crucial to the algorithm's effectiveness. Finally, other algorithms that will be used for comparison with the developed algorithm are also introduced.

4.1. The proposed framework

To begin, some fundamental concepts are introduced in a brief way. Let's assume there is a feasible solution

set denoted as $\boldsymbol{X} = \{X_1, \cdots, X_i, \cdots, X_n\}$. The objective function value of the ith solution X_i in set $\boldsymbol{X}$ can be represented as $f(X_i) = [f_1(X_i), \cdots, f_j(X_i), \cdots, f_m(X_i)]$, where m is equal to 3 in this paper. In the context of Pareto dominance theory, if one solution X_a dominates one solution X_b ($X_a \prec X_b$), it follows that $\forall j \in \{1,2,\cdots,m\}$: $f_j(X_a) \leq f_j(X_b)$ and $\exists j \in \{1,2,\cdots,m\}$: $f_j(X_a) < f_j(X_b)$. Consequently, a Pareto-dominant ranking emerges. Solutions within the same Pareto-dominant ranking do not mutually dominate each other. Dominating relationships exist between solutions in different Pareto-dominant rankings. If X_i cannot be dominated by any solutions in set $\boldsymbol{X}$, it possesses the highest Pareto-dominant ranking and can be termed a Pareto optimal solution. The set containing all Pareto optimal solutions is referred to as the PF.

Fig. 4 delineates the novel methodology framework employed in this study, which encapsulates both the principal procedural steps and the developed multi-objective solution algorithm.

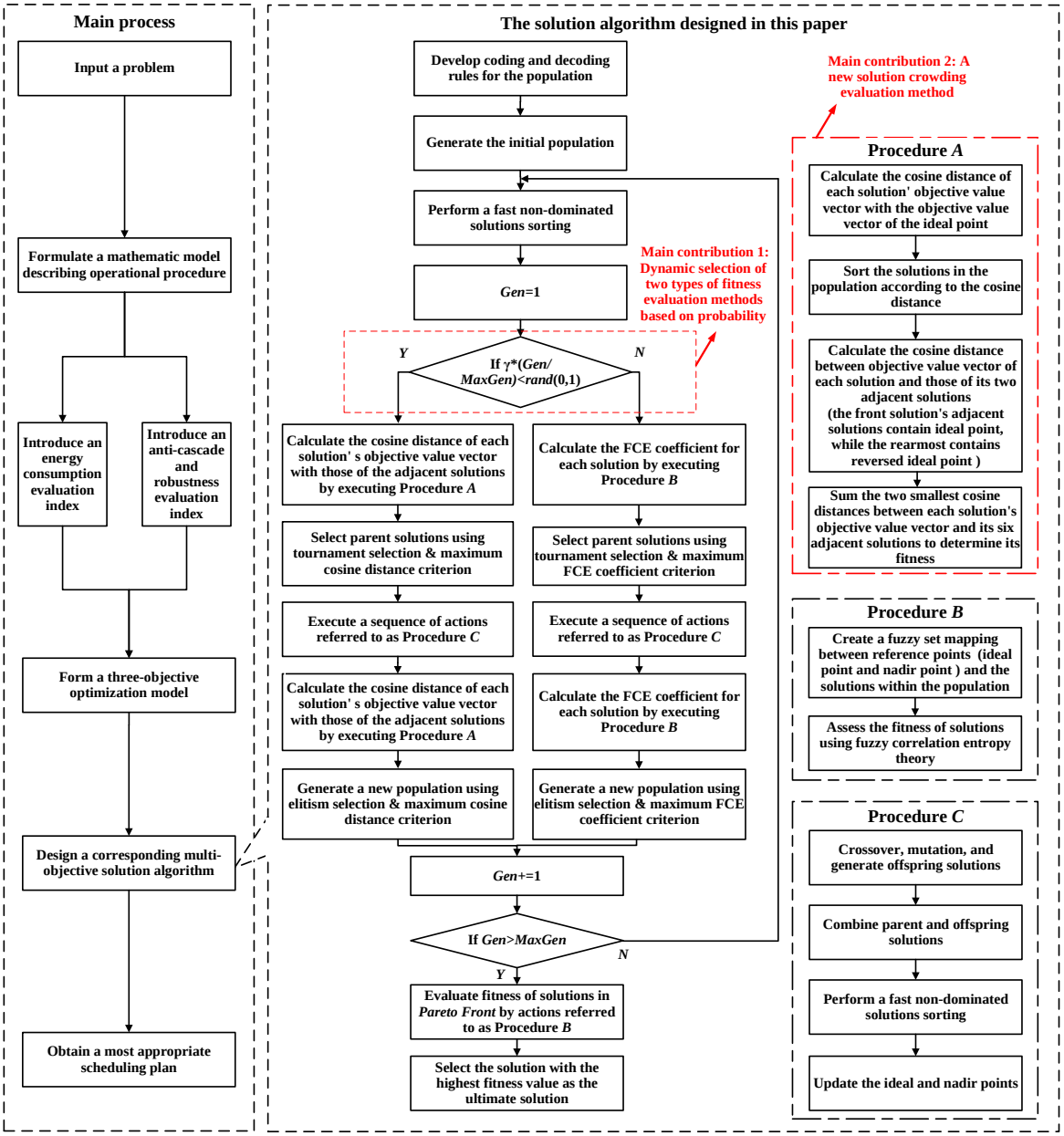

Fig. 4. The framework of the methodology.

In the main process of the methodology framework, an energy consumption calculation index for energy efficiency, as well as an anti-cascade effect and robustness evaluation index, which assesses the schedule's resilience amid uncertain operation times, are integrated into a comprehensive mathematical model that

epitomizes operational efficiency. Subsequently, the tri-objective optimization model is resolved by a multi-objective solution algorithm, thereby acquiring a suitable scheduling plan.

During the solution selection process, it is evident that solutions with higher Pareto-dominant rankings should be prioritized. In NSGA-II, when solutions have the same Pareto-dominant ranking, preference is given to those with a greater crowding distance. Although this approach can aid in maintaining population diversity to some extent, it could not fully reflect the crowding degree of the entire population. Moreover, focusing solely on the crowding distance does not effectively differentiate between superior and inferior solutions, particularly when it comes to selecting the most suitable solution among those sharing the same ranking within the PF. To address this challenge, this paper makes two main contributions to the development of a novel multi-objective solution algorithm. The first contribution of this algorithm is the design of a dynamic selection mechanism for fitness evaluation operators. In the early stages of iterations, the new crowding distance evaluation is more frequently employed to enhance population diversity. As the iterations progress to the later stages, the FCE operator is predominantly used to facilitate rapid convergence and select more suitable solutions. The second contribution is the introduction of a new crowding distance operator based on the cosine distance of solutions' objective value vectors, which effectively evaluates the crowding degree across the entire population.

4.2. The developed multi-objective solution algorithm

The main procedures of the developed algorithm are as follows: Firstly, encoding and decoding rules must be established to generate a feasible population of chromosomes representing the scheduling plan. Next, during each iteration of the population, chromosomes undergo crossover and mutation to produce an offspring population with improved fitness.

Importantly, in the early stages of the algorithm's iterations, the novel crowding distance evaluation is utilized to select the most suitable solution with large objective value vector cosine distances, thereby guaranteeing solution diversity. In the middle and latter stages of the algorithm's iterations, the FCE coefficient is employed to facilitate rapid convergence and the selection of suitable solutions. Here, as described in main contribution 1, a dynamic fitness evaluation method selection mechanism is designed. The selection condition is based on the formula: if selection threshold $\gamma * (Gen/MaxGen)$, where γ is the amplification coefficient, *Gen* is the current generation index, and *MaxGen* is the maximum number of generations, is less than a randomly generated number between 0 and 1, then the crowding distance fitness evaluation will be selected; otherwise, the FCE coefficient fitness evaluation will be selected. As the number of generations increases, the selection threshold will also increase, making the selection of the FCE coefficient fitness evaluation more likely. This approach ensures that as the solution process progresses, the algorithm shifts focus from exploring diversity to converging on more optimal solutions. Ultimately, when the maximum number of iterative generations is reached, the solution from the PF with the highest fitness value, as determined by the FCE coefficient, is selected as the final solution.

4.2.1. Encoding and decoding

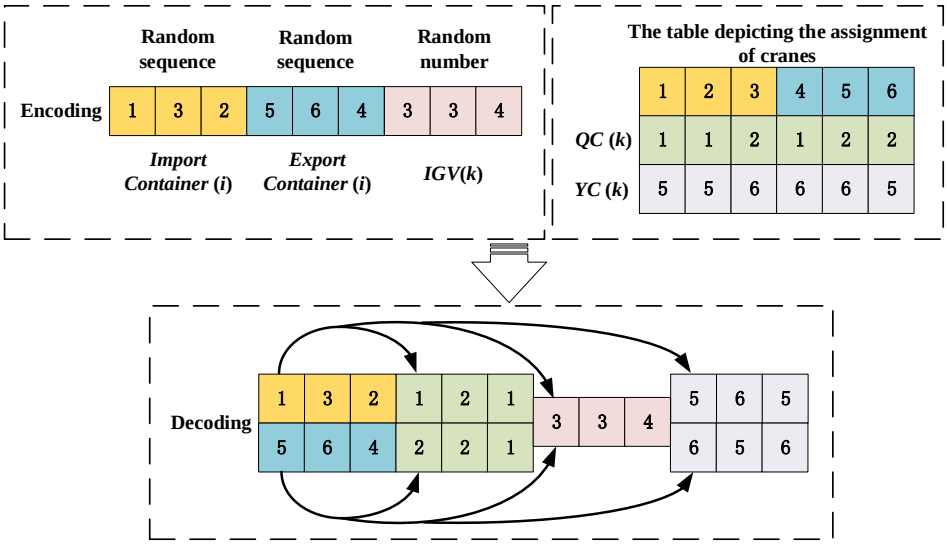

Fig. 5. The process of encoding and decoding the chromosome.

Fig. 5 illustrates the encoding and decoding rules in detail. During the encoding phase, the index numbers of import and export containers are subjected to a random permutation, while the index numbers of IGVs are generated randomly as well. The number of IGV indices in a chromosome equals the count of import or export container indices. This establishes a one-to-one correspondence between an IGV and an import-export container pair, forming a double-cycling operation scheme.

Decoding involves the utilization of a reference table that maps the pre-assigned cranes to the containers they handle. For instance, as depicted in Fig. 5, consider the import container 1. Initially, QC 1 unloads it from the shoreline onto IGV 3. Subsequently, IGV 3 transports it from the shoreline to the yard area. Finally, YC 5 loads it from IGV 3 onto a designated yard slot. After completing the import container 1 task, IGV 3 proceeds to handle export container 5 in coordination with YC 6, exemplifying the double-cycling operation.

Notably, the sequencing rules for tasks within the equipment, as depicted in Fig. 5, are governed by a column-first and then row-first pattern. As an example, QC 1 starts by unloading import container 1, followed by the handling of import container 2 and export container 4. Similarly, YC 5's sequence begins with loading import container 1, then unloading export container 6, and finally loading import container 2. This systematic approach generates a viable scheduling plan that adheres to the operational constraints.

4.2.2. Crossover and mutation

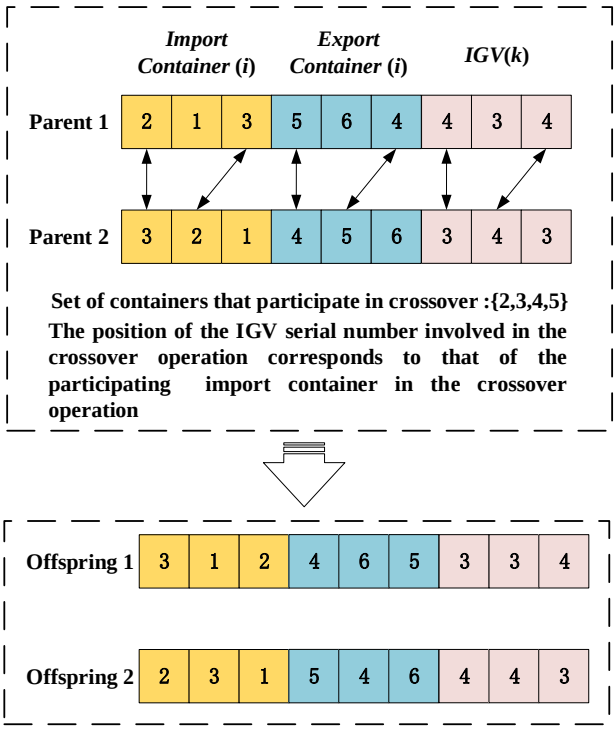

Fig. 6. The process of crossing over the chromosome.

The corresponding segments of containers of the same type or the IGVs from the two parent chromosomes can undergo crossover. There is a probability of crossover for the chromosome segment consisting of import containers and export containers. Firstly, the serial numbers of the containers participating in the crossover operation will be randomly generated to form a crossover set. For instance, as shown in Fig.6, the containers selected for the crossover operation are numbers 2, 3, 4, and 5. Here, containers 2 and 3 represent the import containers, while containers 4 and 5 signify the export containers. Then, the serial numbers of containers in the parent 1 chromosome that are also in the set will be crossed with those in parent 2. During the crossover, the relative order of the serial numbers of containers participating in the crossover operation within the parent chromosome will remain unaltered (refer to Fig. 6). To ensure the feasibility of the chromosome, the positions of the IGVs chromosome segment participating in the crossover operation will be aligned with those of the imported containers.

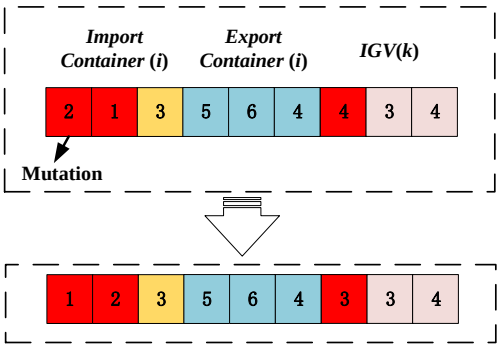

Fig. 7. The process of mutating the chromosome.

The chromosome mutation probability is typically set to a low value, and the mutation scope is limited. Each type of container and IGV has a probability of mutation. For segments of the chromosome corresponding to import containers or export containers, two mutation positions will be randomly selected.

These two positions will then swap (as depicted in Fig. 7). When segments of the chromosome corresponding to IGVs mutate, the serial number of the IGV at the mutation position will be replaced with another random number (as shown in Fig. 7).

Both crossover and mutation operations are essential components of the developed evolutionary algorithm. After several iterations, chromosomes with higher fitness will be selected and evolved.

4.2.3. Dynamic reference points

Reference points play a crucial role both in calculating the crowding distance and the FCE coefficient. In conventional approaches, both ideal and nadir points must be established beforehand, typically determined at their optimal values. However, this approach has notable drawbacks; it necessitates conducting single-objective optimizations to identify these points, a procedure that is both laborious and time-consuming. This challenge is exacerbated in the context of complex and large-scale issues. Consequently, this paper introduces a dynamic approach for adjusting ideal and nadir points, which allows for their variation with each generation during the iterative process. The ideal point vector represents the best values of all objectives achieved across previous generations, while the nadir point vector denotes the worst values. Both the ideal and nadir points are dynamically updated at each iteration. This approach is particularly beneficial for addressing large-scale problems and has been proven effective in enhancing solution quality and reducing computational time, as evidenced by (He et al., 2022).

Specifically, the reference points encompass the dynamic ideal point, X_{IP}, and the dynamic nadir point, X_{NP}. In a specific generation g, the ideal point and nadir point are represented as X_{IP}^{g} and X_{NP}^{g}, respectively. Let ${f_j^g}_{min}$ and ${f_j^g}_{max}$ denote the optimal and worst values of optimization objective j within the feasible solution set $\boldsymbol{X}^g$ in generation g. Consequently, the multi-objective function values of the ideal point in generation g can be expressed as $X_{IP}^{g} = [min({f_1^1}_{min}, \cdots, {f_1^g}_{min}), \cdots, min({f_j^1}_{min}, \cdots, {f_j^g}_{min}), \cdots, min({f_m^1}_{min}, \cdots, {f_m^g}_{min})]$, and the multi-objective function values of the nadir point in generation g can be represented as $X_{NP}^{g} = [max({f_1^1}_{max}, \cdots, {f_1^g}_{max}), \cdots, max({f_j^1}_{max}, \cdots, {f_j^g}_{max}), \cdots, max({f_m^1}_{max}, \cdots, {f_m^g}_{max})]$. These reference points evolve throughout the iterative process, updating in each generation.

4.2.4. Crowding degree evaluation based on cosine distance of objective value vectors

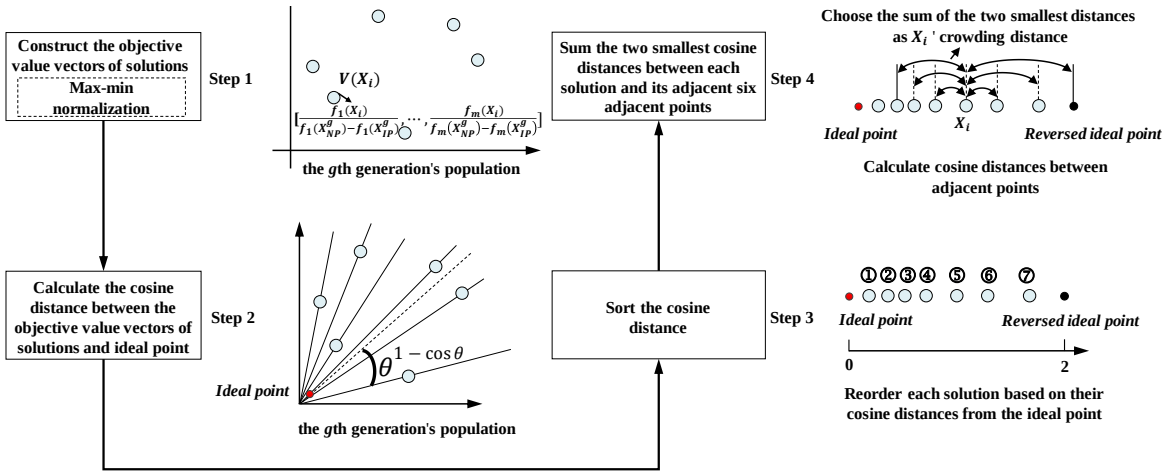

Fig. 8. The calculation process for crowding degree based on the cosine distance of objective value vectors.

The crowding degree evaluation method based on the cosine distance of objective value vectors enables to

compare the cosine distance between each solution and its adjacent solutions. The order of solutions is determined by their cosine distances from the ideal point. This method addresses the limitations of the traditional crowding degree evaluation method in NSGA-II, which does not reflect the crowding degree from the perspective of the entire population. Fig. 8 illustrates the four main steps of this method.

1) Constructing the objective value vectors for each solution

This step aids in transforming each solution into a vectorized point based on its objective values, facilitating the calculation of cosine distance in subsequent steps. A max-min normalization method is employed to normalize each objective value vector for each solution. The objective value vector of solution X_i, denoted as $V(X_i)$, is defined in Eq. (51).

$$V(X_i)=\left[\frac{f_1(X_i)}{f_1(X_{NP}^g)-f_1(X_{IP}^g)},\cdots,\frac{f_j(X_i)}{f_j(X_{NP}^g)-f_j(X_{IP}^g)},\cdots,\frac{f_m(X_i)}{f_m(X_{NP}^g)-f_m(X_{IP}^g)}\right]=[f'_1(X_i),\cdots,f'_j(X_i),\cdots,f'_m(X_i)] \quad (51)$$

Here, $f_j(X_{NP}^g)$ and $f_j(X_{IP}^g)$ represent the jth objective value of solution X_i, the nadir point and ideal points in the gth generation, respectively.

2) Calculating the cosine distance between each solution's objective vector and the ideal point's

This step involves calculating the cosine distance between each solution's objective vector and the ideal point vector in the gth generation, represented as $D[V(X_i),V(X_{IP}^g)]$. The cosine distance is derived by subtracting the cosine similarity from 1, as defined in Eq. (52).

$$D[V(X_i),V(X_{IP}^g)]=1-\frac{\sum_{j=1}^m f'_j(X_i)\cdot f'_j(X_{IP}^g)}{\sqrt{\sum_{j=1}^m[f'_j(X_i)]^2}\cdot\sqrt{\sum_{j=1}^m[f'_j(X_{IP}^g)]^2}} \quad (52)$$

The larger the cosine angle between a solution's objective vector and the ideal point vector, the greater the resulting cosine distance.

3) Sorting the cosine distance

After calculating the cosine distance, the solutions are ordered in ascending order based on their cosine distance from the ideal point vector.

4) Summing the two smallest cosine distances between each solution vector and its six adjacent points

The developed crowding degree is represented by the sum of the two smallest cosine distances between the solution's objective value vectors and its six adjacent solutions, which are sorted based on their distance from the ideal point. The rationale for selecting six adjacent solutions is to strike a balance between accuracy and computational efficiency. This specific number helps to mitigate scenarios where points adjacent to the target solution in sequence do not correspond to those in a vector space. Choosing a larger number of adjacent solutions increases the likelihood of identifying the true adjacent points but at the cost of extended computation time. Conversely, a smaller number will lead to inaccuracies in identifying these points. Thus, six is tested and validated as a suitable compromise for this study. For the solution vector $V(X_i)$, if its kth preceding point is $V(X_{i-k})$ and the kth subsequent point is $V(X_{i+k})$, the crowding degree of solution X_i, denoted as $C(X_i)$, is calculated by the using Eq. (53):

$$C(X_i)=min\{D[V(X_i),D[V(X_{i-3})],\cdots,D[V(X_i),D[V(X_{i-1})],D[V(X_i),D[V(X_{i+1})],\cdots,D[V(X_i),D[V(X_{i+3})]\}+secondmin\{D[V(X_i),D[V(X_{i-3})],\cdots,D[V(X_i),D[V(X_{i-1})],D[V(X_i),D[V(X_{i+1})],\cdots,D[V(X_i),D[V(X_{i+3})]\} \quad (53)$$

It should be noted that if $V(X_i)$ is among the first three points, its preceding point includes the ideal point, denoted as $X_0=X_{IP}^g$. Conversely, if $V(X_i)$ is among the last three points, its subsequent point includes the reversed ideal point, denoted as $X_n=-X_{IP}^g$.

4.2.5. Fuzzy correlation entropy coefficient

The fitness evaluation mechanism, rooted in FCE, establishes a fuzzy mapping relationship between reference points and solutions, thereby generating a correlation entropy coefficient that accurately reflects the fitness of the solutions. This, in turn, facilitates a comprehensive evaluation in terms of the three objectives. This combination can guarantee solution diversity, augment convergence performance, and enable the convenient and efficient selection of the most fitting solution from the PF.

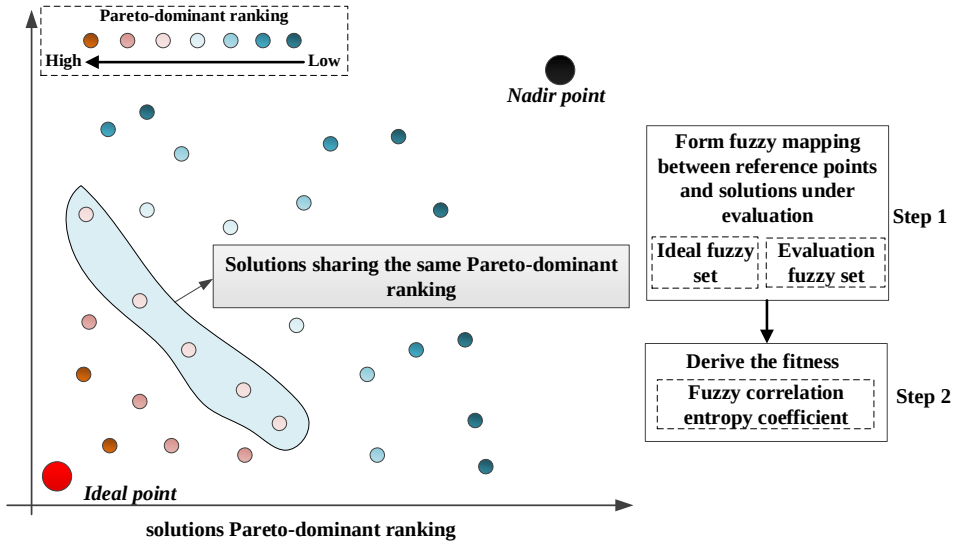

Fig. 9. The calculation process of fuzzy correlation entropy coefficient.

Fig. 9 demonstrates the essential steps of the fitness evaluation method based on FCE, encompassing two crucial steps.

1) Forming the fuzzy mapping relationship

Upon establishing the reference points, the objective values of solutions under assessment can be converted into a fuzzy set in relation to these reference points. The pivotal aspect involves the selection of an appropriate fuzzy membership function. In accordance with the traits of engineering optimization problems, the semi-trapezoidal membership function has been adopted for this purpose within this study. The fuzzy membership value, denoted as $\mu(f_j^g(X_i))$, for the jth objective of the ith solution, X_i, in generation g can be defined by Eq. (54),

$$\mu(f_j^g(X_i)) = \begin{cases} 1, f_j^g(X_i) \le \alpha \cdot f_{jmin}^g \\ \frac{f_j^g(X_i) - \beta \cdot f_{jmax}^g}{\alpha \cdot f_{jmin}^g - \beta \cdot f_{jmax}^g}, \alpha \cdot f_{jmin}^g < f_j^g(X_i) < \beta \cdot f_{jmax}^g \\ 0, f_j^g(X_i) \ge \beta \cdot f_{jmax}^g \end{cases} \tag{54}$$

Here, α and β symbolize the amplification and reduction factors, respectively, with the condition that $0 < \alpha \le 1$ and $\beta > 1$. The rationale behind using α and β is to prevent encountering zero or infinity during entropy calculations.

As a result, the objective values of solution X_i in generation g can be translated into a fuzzy set denoted as $U(f^g(X_i)) = \left\{\mu(f_1^g(X_i)), \cdots, \mu(f_j^g(X_i)), \cdots \mu(f_m^g(X_i))\right\}$. Similarly, following a similar approach, the ideal point in generation g can be represented as a fuzzy set $U(f^g(X_{IP}^g)) = \left\{\mu(f_1^g(X_{IP}^g)), \cdots, \mu(f_j^g(X_{IP}^g)), \cdots \mu(f_m^g(X_{IP}^g))\right\}$.

2) Deriving the fuzzy correlation entropy coefficient

The fuzzy set representing the ideal point encapsulates ideal objective values. The mapping process of the objective values of solutions under evaluation essentially involves comparing these solutions with the ideal point. Through the computation of the FCE coefficient between the fuzzy set of the ideal point $U(f^g(X_{IP}^g))$ and the fuzzy set of objective values of a solution X_i under evaluation $U(f^g(X_i))$, the degree of resemblance between the evaluated solution and the ideal point can be gauged. It can be inferred that a higher FCE coefficient corresponds to a greater degree of similarity, indicating higher fitness of the solution.

The process of calculating the FCE coefficient between $U(f^g(X_{IP}^g))$ and $U(f^g(X_i))$ is as follows:

① Calculate the information entropy $E(\cdot)$ for $U(f^g(X_{IP}^g))$ and $U(f^g(X_i))$ using Eqs. (55) and (56):

$$E[U\left(f^g(X_{IP}^g)\right)] = -\frac{1}{m\cdot\ln(2)}\cdot\sum_{j=1}^{m}\{\mu\left(f_j^g(X_{IP}^g)\right)\cdot\ln\left[\mu\left(f_j^g(X_{IP}^g)\right)\right] + [1-\mu\left(f_j^g(X_{IP}^g)\right)]\cdot \ln\left[1-\mu\left(f_j^g(X_{IP}^g)\right)\right]\} \quad (55)$$

$$E[U(f^g(X_i))] = -\frac{1}{m\cdot\ln(2)}\cdot\sum_{j=1}^{m}\{\mu\left(f_j^g(X_i)\right)\cdot\ln\left[\mu\left(f_j^g(X_i)\right)\right] + [1-\mu\left(f_j^g(X_i)\right)]\cdot\ln\left[1-\mu\left(f_j^g(X_i)\right)\right]\} \quad (56)$$

Here, $\frac{1}{m\cdot\ln(2)}$ represents the normalization factor.

②Calculate the partial entropy of $U(f^g(X_{IP}^g))$ with respect to $U(f^g(X_i))$ using Eq. (57):

$$E_{U(f^g(X_i))}[U\left(f^g(X_{IP}^g)\right)] = -\frac{1}{m\cdot\ln(2)}\cdot\sum_{j=1}^{m}\{\mu\left(f_j^g(X_i)\right)\cdot\ln\left[\mu\left(f_j^g(X_{IP}^g)\right)\right] + [1-\mu\left(f_j^g(X_i)\right)]\cdot \ln\left[1-\mu\left(f_j^g(X_{IP}^g)\right)\right]\} \quad (57)$$

③ Calculate the partial entropy of $U(f^g(X_i))$ with respect to $U(f^g(X_{IP}^g))$ using Eq. (58):

$$E_{U(f^g(X_{IP}^g))}[U(f^g(X_i))] == -\frac{1}{m\cdot\ln(2)}\cdot\sum_{j=1}^{m}\{\mu\left(f_j^g(X_{IP}^g)\right)\cdot\ln\left[\mu\left(f_j^g(X_i)\right)\right] + [1-\mu\left(f_j^g(X_{IP}^g)\right)]\cdot \ln\left[1-\mu\left(f_j^g(X_i)\right)\right]\} \quad (58)$$

④ Calculate the fuzzy correlation entropy $E\left[U\left(f^g(X_{IP}^g)\right), U(f^g(X_i))\right]$ between $U(f^g(X_{IP}^g))$ and $U(f^g(X_i))$ using Eq. (59):

$$E\left[U\left(f^g(X_{IP}^g)\right), U(f^g(X_i))\right] = E_{U(f^g(X_i))}\left[U\left(f^g(X_{IP}^g)\right)\right] + E_{U(f^g(X_{IP}^g))}[U(f^g(X_i))] \quad (59)$$

⑤ Calculate the fuzzy correlation entropy coefficient $\rho\left[U\left(f^g(X_{IP}^g)\right), U(f^g(X_i))\right]$ between $U(f^g(X_{IP}^g))$ and $U(f^g(X_i))$ using Eq. (60):

$$\rho\left[U\left(f^g(X_{IP}^g)\right), U(f^g(X_i))\right] = m\cdot\ln(2)\frac{E\left[U\left(f^g(X_{IP}^g)\right)\right]+E[U(f^g(X_i))]}{E\left[U\left(f^g(X_{IP}^g)\right), U(f^g(X_i))\right]} \quad (60)$$

The range of $\rho\left[U\left(f^g(X_{IP}^g)\right), U(f^g(X_i))\right]$ is $0 \le \rho\left[U\left(f^g(X_{IP}^g)\right), U(f^g(X_i))\right] = \rho\left[U(f^g(X_i)), U\left(f^g(X_{IP}^g)\right)\right] \le 1$. Only when $U\left(f^g(X_{IP}^g)\right) = U(f^g(X_i))$, $\rho\left[U\left(f^g(X_{IP}^g)\right), U(f^g(X_i))\right] = \rho\left[U(f^g(X_i)), U\left(f^g(X_{IP}^g)\right)\right] = 1$.

Hence, this method quantifies the similarity between the solution under evaluation and the ideal point by calculating their fuzzy correlation entropy coefficient ρ. This coefficient can be interpreted as the fitness of the solution. Larger ρ values indicate better solutions.

4.3. Comparative methods

Five comparative methods are employed to assess the performance of our developed algorithm, the Multi-objective Genetic Algorithm incorporating Cosine Distance and FCE (MoGA-CoD-FCE). This assessment emphasizes MoGA-CoD-FCE's superiority in terms of operational efficiency, energy efficiency, and scheduling robustness.

4.3.1. Traditional single-objective optimization focusing on minimizing *makespan*

In a traditional container terminal, optimizing the *makespan* is a common objective. However, focusing solely on *makespan* optimization may lead to schedules that lack robustness and energy efficiency. It is important to note that the differences between single-objective optimization and multi-objective optimization, as well as their respective effects on the schedule, are not known until comparative experiments are conducted. Therefore, in this study, the Traditional Single-objective Genetic Algorithm (TSGA) with *makespan* as the optimization objective is chosen for experimental comparison.

4.3.2. Weighted multi-objective genetic algorithm

The linear weighted summation of multiple objective functions can transform a multi-objective optimization problem into a single-objective optimization problem, offering a scalar-based approach to multi-objective optimization. However, the selection of rational weight values is crucial in practical applications. In this paper, we have set the weighted values for *makespan* (w_1), *energy consumption* (w_2), and *robustness* (w_3) as follows: 0.43, 0.33, and 0.24, respectively. Operational efficiency takes precedence in importance, followed by energy consumption, aligning with the actual priorities of the port.

Nevertheless, due to the diverse units and dimensions of each objective function value, further transformation of the weighted objective function is required. The widely recognized normalization approach, $\frac{f_j^g(X_i)-f_{jmin}^g}{f_{jmax}^g-f_{jmin}^g}, \forall j = 1,2,3$, although frequently cited in literature such as Zhu et al. (2018), which focuses on multi-objective optimization based on Pareto domination, encountered stability issues in our preliminary experiments. Specifically, the fitness value of the best solution in each generation would fluctuate and fail to converge when this method was applied in such a scalar-based approach to multi-objective optimization. To address this, some researchers, like Ji et al. (2019), have adopted a constant to normalize the objective function values by dividing $f_j^g(X_i)$. In this study, we opt for a practical and straightforward approach by using the minimum objective value from the first generation, formulated as $\frac{f_j^g(X_i)}{f_{jmin}^g}, \forall\ j = 1,2,3$. Consequently, let $fitness^g(X_i)$ represent the fitness value of feasible solution X_i in set $\boldsymbol{X}^g$ in generation g. The $fitness^g(X_i)$ is defined by Eq. (61):

$$fitness^g(X_i) = w_1 \cdot \frac{f_1^g(X_i)}{f_{1min}^1} + w_2 \cdot \frac{f_2^g(X_i)}{f_{2min}^1} + w_3 \cdot \frac{f_3^g(X_i)}{f_{3min}^1}, \forall X_i \in \boldsymbol{X}^g \tag{61}$$

By dividing each objective's value by the minimum value of that objective in the first generation, the influence of different units and dimensions can be eliminated. Consequently, a smaller fitness value indicates a higher fitness level for the solution in this Weighted Multi-objective Genetic Algorithm (WMGA).

4.3.3. NSGA-II

The NSGA-II algorithm, a prominent representative of optimization techniques based on Pareto dominance, is known for its efficiency and practicality (Cai et al., 2024). However, NSGA-II presents challenges due to its simplistic solution fitness evaluation and difficulty in selecting the most suitable solution from a PF. This

is why our paper introduces a developed algorithm that incorporates a new crowding distance evaluation method and the FCE. To demonstrate the superiority of our developed algorithm, NSGA-II is chosen as a comparative method. In this paper, the function (62) is employed as a means to select an appropriate solution from a PF, which is a widely used approach.

$$Distance(X_i) = \sqrt{[w_1 \cdot \frac{f_1(X_i)-f_{1min}}{f_{1max}-f_{1min}}]^2 + [w_2 \cdot \frac{f_2(X_i)-f_{2min}}{f_{2max}-f_{2min}}]^2 + [w_3 \cdot \frac{f_3(X_i)-f_{2min}}{f_{2max}-f_{2min}}]^2}, \forall X_i \in \mathbf{PF} \quad (62)$$

Eq. (62) calculates the weighted Euclidean distance, eliminating differences in dimension between the objective values of solution X_i and the ideal point in the PF. The solution within the PF with the shortest distance is selected as the final solution, representing the solution closest to the ideal point.

4.3.4. Multi-objective genetic algorithm incorporating FCE

The Multi-objective Genetic Algorithm incorporating FCE (MoGA-FCE) has been utilized in recent studies, such as He et al. (2022) and Wang et al. (2023). This algorithm substitutes the traditional fitness evaluation operator, such as the crowding distance in NSGA-II, with the FCE operator. In their research, MoGA-FCE is shown to outperform renowned multi-objective optimization algorithms like multi-objective differential evolution, multi-objective particle swarm optimization, and NSGA-III. Differing from MoGA-FCE, our developed MoGA-CoD-FCE integrates a dynamic fitness evaluation method selection mechanism, which includes a new crowding distance operator designed to enhance population diversity in the early stage of iterations. Comparing our developed algorithm with this latest and effective algorithm allows for a comprehensive assessment of the developed MoGA-CoD-FCE's performance.

4.3.5. Multi-objective genetic algorithm incorporating traditional crowding distance and FCE

The difference between this Multi-objective Genetic Algorithm incorporating Traditional Crowding Distance and FCE (MoGA-TCrD-FCE) and our developed algorithm lies in the crowding distance operator. MoGA-TCrD-FCE utilizes a traditional crowding degree operator from NSGA- II, while MoGA-CoD-FCE employs a newly developed crowding degree operator based on a cosine distance. This comparison is designed to evaluate the effectiveness of the newly introduced crowding distance operator, which represents the main contribution 2 of our developed algorithm.

5. Experimental results analysis, discussion, and implication

In this section, the experimental parameters are introduced, derived from real port cases based on our comprehensive survey, and the experimental results are also shown. Then, a discussion and the implications drawn from the experimental results are presented.

5.1. Experiments

5.1.1. Experimental setting

The experimental input parameters, including the traveling distances between loading/unloading points, crane hoisting times, horizontal equipment movement speeds, equipment unit energy consumption, and more, have been sourced from real ports as part of our comprehensive survey.

Table 4. Case parameters.

Parameter	Value	Parameter	Value
Loading/Unloading time of crane	*Normal distribution* $(80,\ {\sigma_1}^2)$ (s)	Horizontal moving speed of crane	*Normal distribution* $(4.2,\ {\sigma_2}^2)$ (m/s)
Horizontal moving speed of IGV	*Normal distribution* $(5.7,\ {\sigma_3}^2)$ (m/s)	Energy consumption of crane during idle periods	2 $(kW{\cdot}h)$
Energy consumption of IV during idle periods	1 $(kW{\cdot}h)$	Energy consumption of crane during loading and unloading operations	11 $(kW{\cdot}h)$
Energy consumption during crane horizontal	15 $(kW{\cdot}h)$	Energy consumption during IV horizontal movement without a	14 $(kW{\cdot}h)$

movement without a load		load	
Energy consumption during IV horizontal movement with a load	21 ($kW{\cdot}h$)	Maximum number of import and export containers	2000
Maximum number of QCs	3	Maximum number of YCs	2
Maximum number of IGVs	72		

In addition to the parameters related to the real port cases shown in Table 4, Table 5 presents the parameters related to the algorithms.

Table 5. Algorithm parameters.

Parameter	Value	Parameter	Value
α in MoGA-CoD-FCE, MoGA-TCrD-FCE and MoGA-FCE	0.9	w_1 in WMGA, NSGA-II	0.43
β in MoGA-CoD-FCE, MoGA-TCrD-FCE and MoGA-FCE	1.1	w_2 in WMGA, NSGA-II	0.33
γ in MoGA-CoD-FCE	4	No. of chromosomes within a population	300
w_3 in WMGA, NSGA-II	0.24	The probability of chromosomes crossover	0.5
The probability of chromosome mutation	0.1	No. of evolutionary generations	1000-2500

The experiments were carried out using MATLAB R2022a on a Personal Computer (PC) equipped with an Intel i9-11900 2.50GHz processor and 32 GB of RAM.

5.1.2. Experimental results

To ensure a valid and equitable comparison, all the methods utilized identical coding, decoding, crossover, and mutation rules for their respective populations. Furthermore, the parameters governing the evolutionary generations, the population size, and the weight coefficients for the optimization objectives were configured consistently across the different methods.

Once the most appropriate pre-scheduling plans have been chosen using each method, they will undergo execution within a simulated environment encompassing uncertain operation times. This uncertainty is classified into four levels in each case. Within each level of uncertainty for each case, the pre-scheduling plan will be executed 20,000 times, and the resultant average values will be presented in Table 6.

924 **Table 6**. Average objective values from 20,000 experiments and CPU computation times obtained using six methods.

Case scale	Uncertainty ($\sigma_1^2 - \sigma_2^2 - \sigma_3^2$)	TSGA			WMGA			NSGA-II			MoGA-FCE			New Algorithm					
														MoGA-TCrD-FCE			MoGA-CoD-FCE		
		Makespan (s)	*Energy (kW·h)*	*CPU Time(s)*	*Makespan (s)*	*Energy (kW·h)*	*CPU Time(s)*	*Makespan (s)*	*Energy (kW·h)*	*CPU Time(s)*	*Makespan (s)*	*Energy (kW·h)*	*CPU Time(s)*	*Makespan (s)*	*Energy (kW·h)*	*CPU Time(s)*	*Makespan (s)*	*Energy (kW·h)*	*CPU Time(s)*
Case 1 (8/8/1/3/2)	5-0.04-0.3	**3761.6**	20.2	**106.9**	3762.3	18.8	148.4	3762.2	**18.5**	169.9	3762.4	18.8	231.6	3762.5	18.8	250.5	3761.8	18.8	198.3
	10-0.08-0.6	3772.6	20.0	**136.6**	3772.4	19.7	168.6	**3771.6**	18.7	159.6	3773.0	17.9	172.9	3771.8	**17.9**	160.6	3772.3	17.9	160.9
	15-0.12-0.9	3791.7	20.6	**141.8**	**3789.2**	19.8	176.6	3791.8	18.7	151.6	3790.3	19.8	207.5	3790.9	18.0	161.6	3790.8	**18.0**	157.1
	20-0.15-1.2	3821.2	20.9	**118.1**	3820.5	20.0	157.4	3821.6	19.0	154.5	**3819.8**	**18.2**	170.8	3821.0	18.2	154.7	3821.8	20.0	188.0
Case 2 (15/15/2/5/2)	5-0.04-0.3	3645.9	36.4	**251.7**	3664.4	36.2	286.1	3575.1	**34.6**	268.5	**3568.1**	34.7	268.5	3655.3	34.9	273.1	3656.8	34.9	267.3
	10-0.08-0.6	3596.9	36.8	**196.1**	**3593.7**	36.4	237.8	3672.1	35.6	269.9	3758.9	**35.5**	270.2	3594.1	37.4	259.5	3594.0	37.3	263.1
	15-0.12-0.9	3725.2	37.2	**196.6**	**3625.2**	36.6	235.1	3755.3	35.4	257.4	3722.0	36.7	268.5	3707.9	36.1	266.9	3688.5	**35.2**	265.5
	20-0.15-1.2	3673.1	37.2	**194.6**	3802.1	38.3	231.7	3789.8	38.5	242.9	3801.4	37.5	251.7	3675.8	37.5	256.3	**3667.6**	**36.1**	254.7
Case 3 (30/30/2/7/2)	5-0.04-0.3	7012.2	72.2	489.6	7408.3	72.3	585.2	7019.0	65.1	517.1	**6952.3**	66.0	507.2	6962.9	**61.5**	**465.9**	7031.6	66.6	494.2
	10-0.08-0.6	6991.3	71.3	537.7	7171.9	72.8	609.7	7060.9	67.4	480.6	**6955.5**	61.2	434.7	6956.5	**59.4**	425.9	6979.7	60.8	**411.9**
	15-0.12-0.9	7060.8	74.5	542.5	7292.6	72.2	603.1	7226.8	68.1	477.0	7072.0	67.9	507.9	7067.8	**61.6**	**416.7**	**6983.3**	61.8	423.1
	20-0.15-1.2	7156.2	73.3	504.3	7701.8	74.7	589.7	7308.4	67.8	537.2	7157.5	68.6	518.4	**7141.0**	**59.6**	431.5	7196.5	61.8	**425.6**
Case 4 (60/60/2/20/2)	5-0.04-0.3	13328	170.1	1262	14157	164.0	1506	13347	155.4	1138	12937	122	**1031**	12905	122	1077	**12828**	**121**	1755
	10-0.08-0.6	**12889**	167.6	1304	13876	157.2	1714	13607	158.0	1360	12923	125	1036	12905	**121**	**995**	12941	123	1688
	15-0.12-0.9	13091	168.6	1407	14196	159.6	1888	13429	153.5	1620	13154	128	1020	13232	**125**	**998**	**12966**	126	1679
	20-0.15-1.2	**13197**	170.1	1434	14642	161.7	2305	13838	156.4	1541	13333	128	1012	13334	126	**1003**	13207	**124**	1689
Case	5-0.04-0.3	21047	323.9	3575	23708	321.8	3579	22783	301.6	**2225**	**20299**	213	2570	20313	221	2635	20437	**212**	2553

5 (100/ 100/ 2/35/ 2)	10-0.08-0.6	21065	336.4	3363	24082	314.2	3367	22410	303.6	**2146**	20601	212	2547	20689	212	2614	**20449**	**207**	2628
	15-0.12-0.9	21278	339.4	3511	22990	308.6	3425	23038	322.2	**2239**	**20639**	213	2511	20694	214	2521	20880	**211**	2557
	20-0.15-1.2	21550	343.6	3389	23706	323.2	3370	22928	320.3	**2151**	20846	**216**	2540	20922	222	2575	**20806**	220	2554
Case 6 (250/ 250/ 3/45/ 2)	5-0.04-0.3	35551	840	11456	43705	908	13125	38333	864	7666	30039	637	7410	30574	633	7395	**29364**	**625**	**7210**
	10-0.08-0.6	35912	846	11396	43290	893	13022	38076	845	7634	30820	637	7404	30468	636	**7394**	**29579**	**629**	7515
	15-0.12-0.9	36397	855	10854	43413	909	10684	37128	832	**6355**	31903	645	7335	31439	**634**	7398	**30784**	636	7308
	20-0.15-1.2	37048	868	11424	44592	909	13082	39012	868	7656	32008	**642**	**7408**	32472	647	7413	**31438**	648	7560
Case 7 (500/ 500/ 3/56/ 2)	5-0.04-0.3	80379	2085	27373	93525	2249	26210	89109	2191	12756	67581	1665	11108	66151	1664	11819	**64607**	**1652**	**11039**
	10-0.08-0.6	80948	2098	27711	91497	2190	26334	84434	2139	12854	67270	1696	**10773**	67261	**1688**	11746	**65914**	1691	11277
	15-0.12-0.9	81798	2118	27643	93942	2247	26155	88264	2186	12765	67996	1701	**11109**	67305	1692	11497	**66502**	**1682**	11197
	20-0.15-1.2	83032	2147	27780	96133	2278	26164	93116	2311	12717	70725	1784	11251	69885	1742	11670	**69526**	**1738**	**11229**
Case 8 (100 0/ 1000/ 3/72/ 2)	5-0.04-0.3	179563	5302	48313	207795	5796	52460	196683	5670	29713	148972	4522	26794	147951	4510	**26370**	**147310**	**4452**	26544
	10-0.08-0.6	178157	5304	44384	207208	5799	48969	195281	5662	27994	150756	4549	**26522**	148210	4497	27522	**146274**	**4456**	27078
	15-0.12-0.9	185880	5486	46475	201588	5770	49563	189148	5520	29324	151687	4589	**26858**	151780	4552	28290	**147072**	**4535**	26862
	20-0.15-1.2	186449	5496	47126	212757	5993	52271	194990	5684	29807	154868	4684	**26606**	**152124**	**4637**	27667	153630	4640	26875
Winning counts		3	0	**8**	3	0	0	1	2	5	6	4	7	2	10	7	**17**	**16**	5
Total number of complete wins		11			3			8			17			19			**38**		

Notes:

Case scale means the number of import containers/ the number of export containers/ the number of QCs/ the number of IGVs/ the number of YCs.

The best results for each objective are indicated in **shade**.

By examining the data presented in Table 6 and Fig. 9, several noteworthy conclusions are derived. As case sizes increase, the superiority of the developed MoGA-CoD-FCE method becomes increasingly evident, surpassing all other methods. For larger cases, when excluding MoGA-CoD-FCE, the MoGA-TCrD-FCE method incorporating the dynamic fitness evaluation mechanism performs best, followed by MoGA-FCE.

Across most scenarios within the small-scale Cases 1-4, the MoGA-CoD-FCE method fails to outperform both the *makespan* and *energy consumption* indicators. Instead, the MoGA-FCE emerges as the top performer in the majority of these small-scale scenarios for *makespan*, while the MoGA-TCrD-FCE excels in terms of *energy consumption*.

Regarding *computation time*, the TSGA, WMGA, and NSGA-II methods require less time in small-scale cases. However, in the context of large-scale Cases 5-8, the MoGA-FCE, MoGA-TCrD-FCE, and MoGA-CoD-FCE methods exhibit a clear advantage. In Cases 7-8, these methods not only achieve up to a 17%-20% improvement in optimization indicators but also reduce computation time by approximately 10%-50%.

To enhance the visual representation of the experimental results, Fig. 9 illustrates line charts depicting the results for the three indicators.

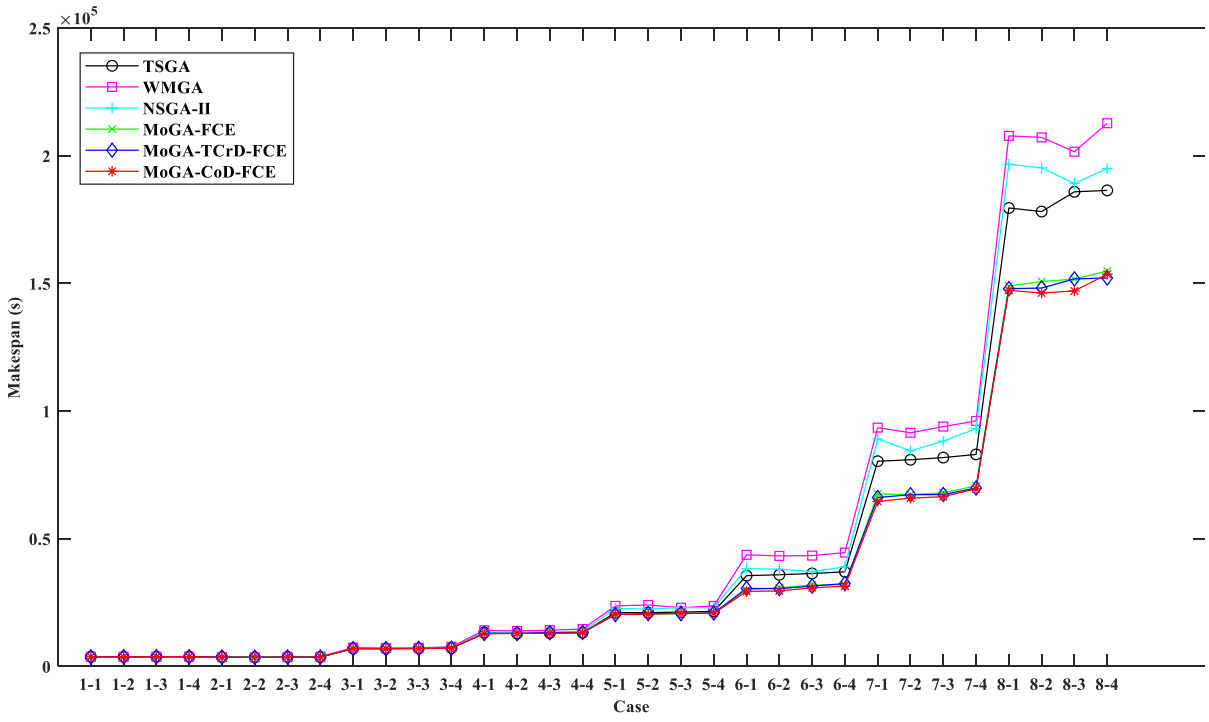

(a) Makespan

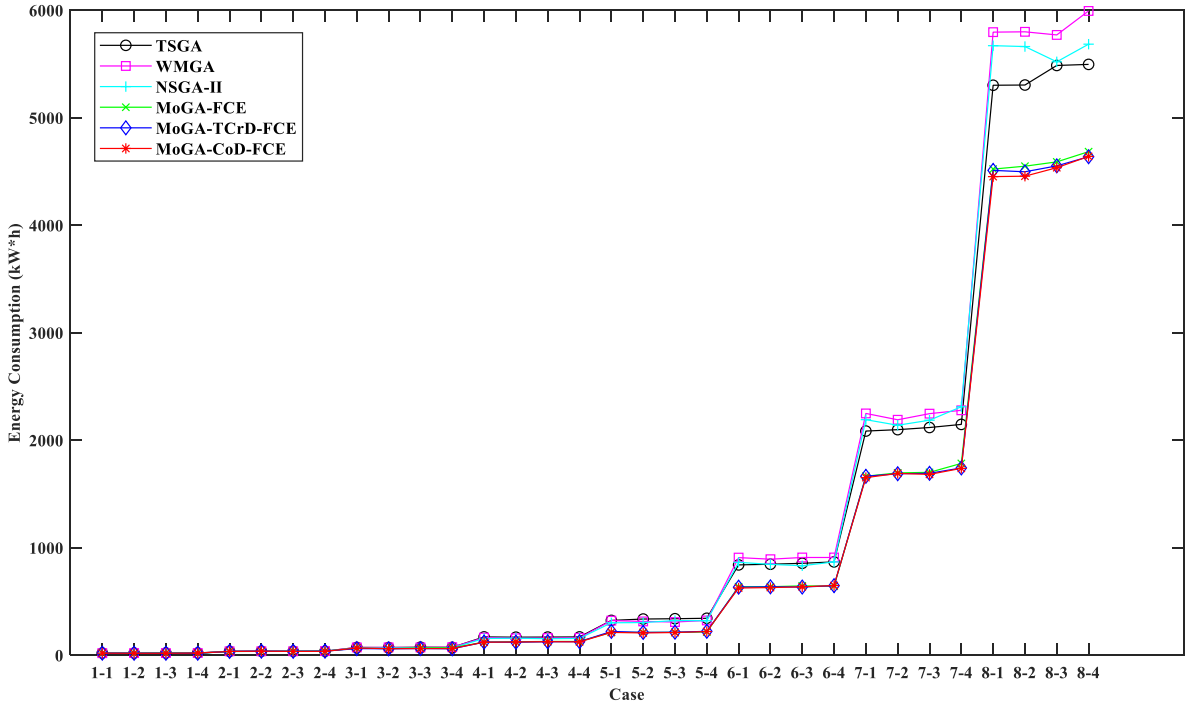

(b) Energy consumption

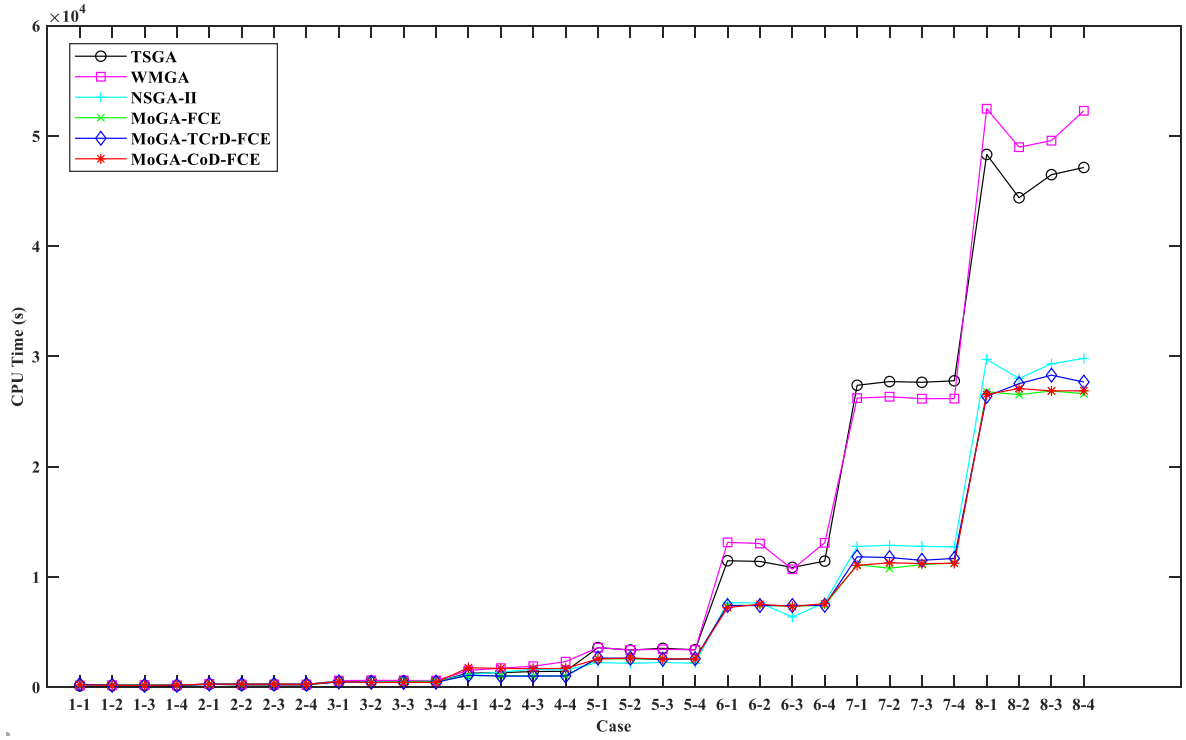

(c) CPU time

Fig. 9. Line charts depicting the experimental results of each method in terms of three indicators.

The three indicators exhibit synchronized trends, particularly in the case of *makespan* and *energy consumption*. Notably, the *computation time* for TSGA and WMGA experience a sudden and sharp increase from Case 5 to Case 8, in contrast to NSGA-II, MoGA-FCE, MoGA-TCrD-FCE, and MoGA-CoD-FCE, as evident in Fig. 9.

In most instances, as the degree of uncertainty increases, there is a consistent deterioration in the *makespan* and *energy consumption* indicators. However, this pattern does not hold for the *computation time* indicator.

For the same cases under varying degrees of uncertainty, the *computation time* for a given method remains consistent.

In conclusion, the analysis of Fig. 8 and Fig. 9 reveals several key findings, 1) The traditional methods, including TSGA, WMGA, and NSGA-II, fail to perform as well as MoGA-FCE, MoGA-TCrD-FCE, and MoGA-CoD-FCE in optimizing *makespan* and *energy consumption* indicators, especially in large cases; 2) Multi-objective optimization algorithms that utilize the Pareto frontier, such as NSGA-II, MoGA-FCE, MoGA-TCrD-FCE, and MoGA-CoD-FCE, can achieve superior optimization results and require less computation time compared to other methods like TSGA and WMGA, particularly in larger cases; Additionally, the newly introduced methods, MoGA-TCrD-FCE and MoGA-CoD-FCE, spent shorter computation times compared to NSGA-II and MoGA-FCE; 3) MoGA-TCrD-FCE and MoGA-CoD-FCE, which incorporate a dynamic fitness evaluation method selection mechanism, outperform existing methods in terms of *makespan* and *energy consumption*, with competitive computation time, especially in large-scale scenarios; 4) The developed MoGA-CoD-FCE, equipped with a dynamic fitness evaluation method selection mechanism and a new crowding distance operator, stands out as the most effective method across all tested optimization indicators and also demonstrates reduced computation time.

5.2. Discussion

The findings of the experimental results demonstrate that the MoGA-TCrD-FCE and MoGA-CoD-FCE methods, incorporating a dynamic fitness evaluation method selection mechanism, outperform other methods. This underscores the effectiveness of the dynamic fitness evaluation method selection mechanism, which is the first contribution of the MoGA-CoD-FCE algorithm. Additionally, the results show that the MoGA-CoD-FCE method, equipped with the new crowding distance operator based on objective value vector cosine distance, surpasses other methods. This highlights the effectiveness of the new crowding distance operator, further demonstrating the second contribution of the MoGA-CoD-FCE algorithm.

To explore the factors underlying the experimental results, additional analyses are conducted. This includes analyzing the three-dimensional PF diagrams for NSGA-II, MoGA-FCE, MoGA-TCrD-FCE, and MoGA-CoD-FCE, monitoring the iterative fitness value curves for TSGA and WMGA, and creating Gantt charts to visualize both the scheduling plans produced by MoGA-CoD-FCE method and the scheduling plans with varying levels of robustness.

5.2.1. Three-dimensional Pareto front diagrams

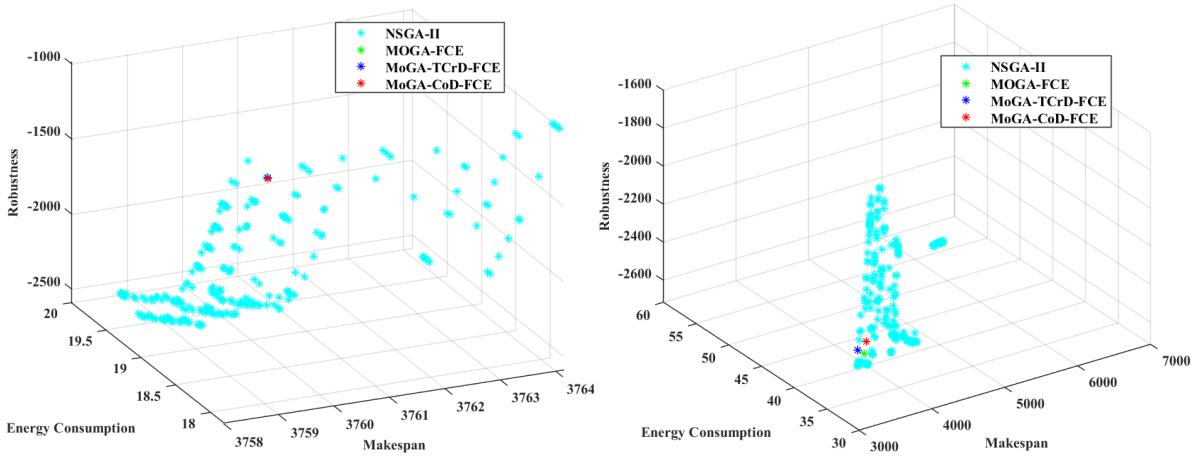

(a) Case 1 (b) Case 2

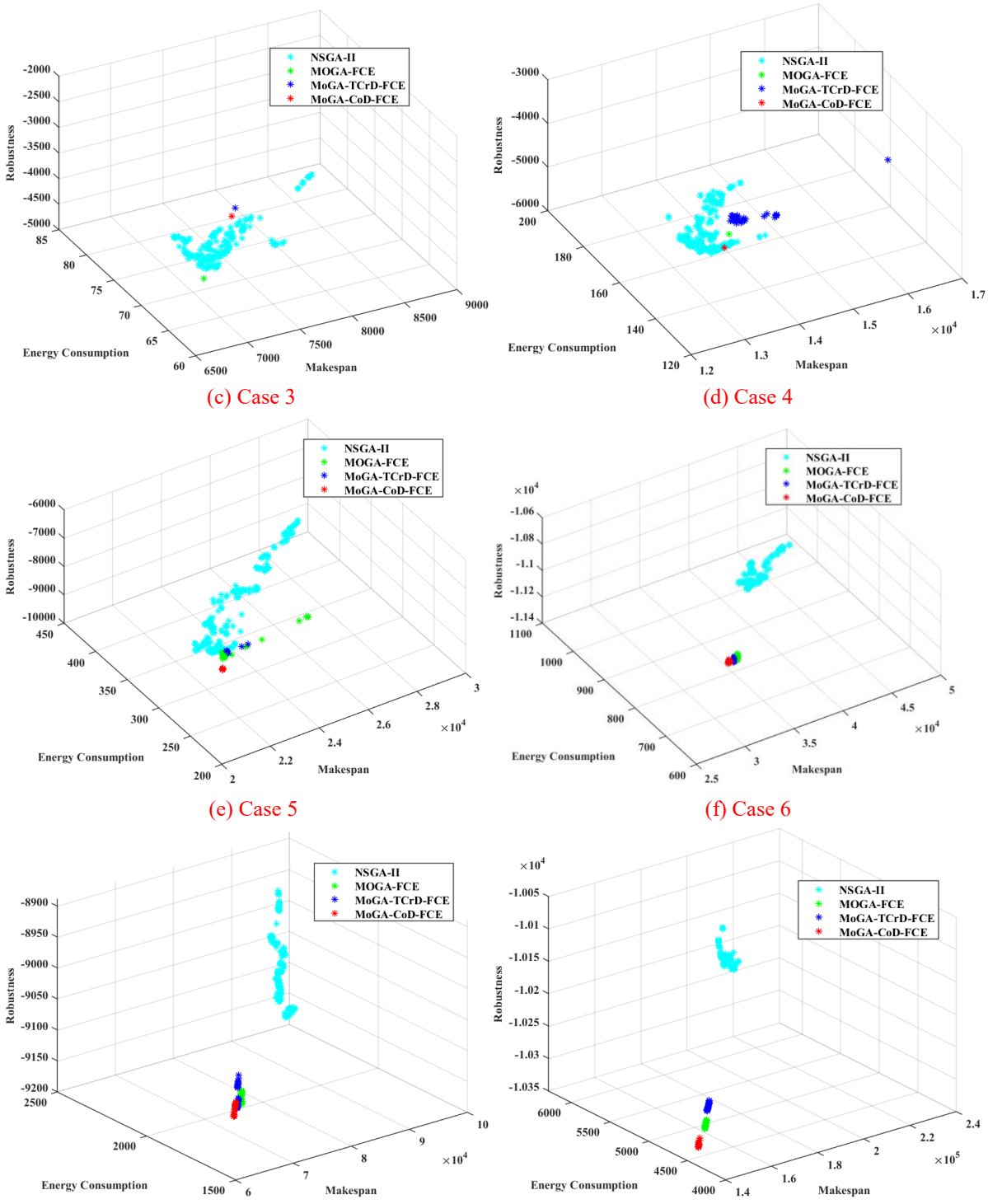

Fig. 10. The three-dimensional Pareto front solutions obtained by four methods.

Fig. 10 presents the PF diagrams generated by NSGA-II, MoGA-FCE, MoGA-TCrD-FCE, and MoGA-CoD-FCE after a specific number of evolutionary iterations. Since each case encompasses four distinct scenarios, each corresponding to a different level of uncertainty, it would be logical to have four diagrams for each case. However, due to the similarity between the diagrams within the same case, one out of every four diagrams has been selected to represent each case. It is evident that the developed MoGA-CoD-FCE exhibits superior performance and effectiveness in large cases. The MoGA-FCE, MoGA-TCrD-FCE, and MoGA-CoD-FCE methods produce a smaller number of solutions within the PF, and these solutions tend to

be closer to the origin of the coordinate system, particularly in large-scale cases. This phenomenon explains why these methods' advantages become more pronounced as the case scale increases. It demonstrates the efficacy of the fitness evaluation method based on FCE employed by MoGA-FCE, MoGA-TCrD-FCE, and MoGA-CoD-FCE. This operator enhances the efficiency of MoGA-FCE, along with the newly introduced MoGA-TCrD-FCE and MoGA-CoD-FCE methods, in identifying superior solutions.

Furthermore, the time complexity of the fitness evaluation mechanism based on the FCE operator is $O[m(logn + 3n)]$, where n and m represent the number of solutions and objectives, respectively. In contrast, the time complexity of the traditional crowding distance operator in NSGA-II is $O(mnlogn)$. Additionally, the time complexity of the newly developed crowding distance operator based on a cosine distance is $O[(m + 6)n + nlogn]$. When the number of objectives is small, the FCE operator demonstrates significantly lower time complexity than the traditional crowding distance operator, explaining why NSGA-II consumes more computation time compared to MoGA-FCE, MoGA-TCrD-FCE, and MoGA-CoD-FCE. Moreover, when the number of solutions is large, the time complexity of the developed crowding distance operator is less than that of the traditional operator, which accounts for the lower computation time observed in MoGA-CoD-FCE and MoGA-FCE compared to MoGA-TCrD-FCE.

In each generation of TSGA and WMGA, fitness values must be calculated twice, once for the parent population and once for the offspring population. In contrast, in each generation of NSGA-II, MoGA-FCE, MoGA-TCrD-FCE, and MoGA-CoD-FCE, fitness values are computed only once due to the Pareto ranking mechanism. This leads to a significant increase in computation time for TSGA and WMGA in large-scale cases.

5.2.2. Iterative fitness value curves

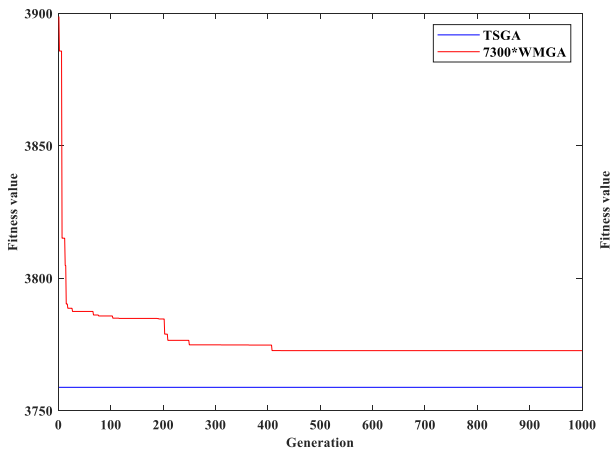

(a) Case 1

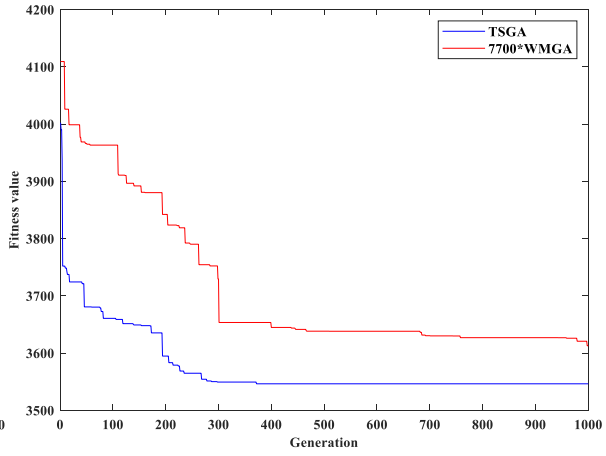

(b) Case 2

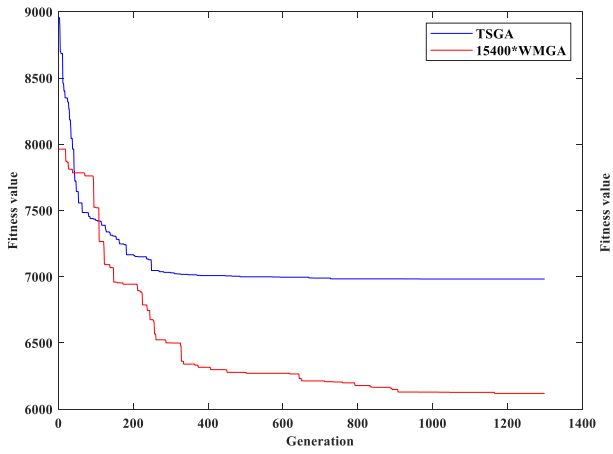

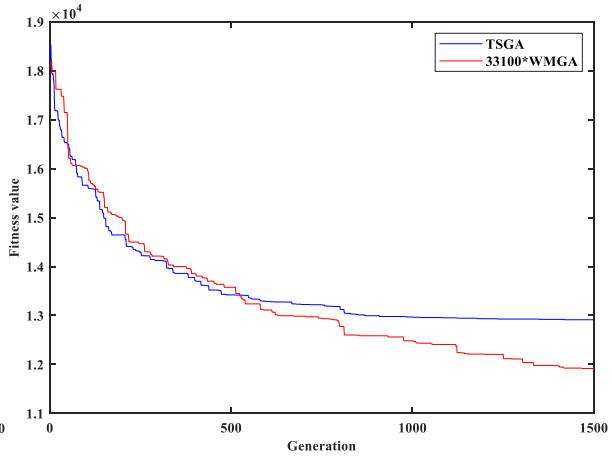

(c) Case 3 (d) Case 4

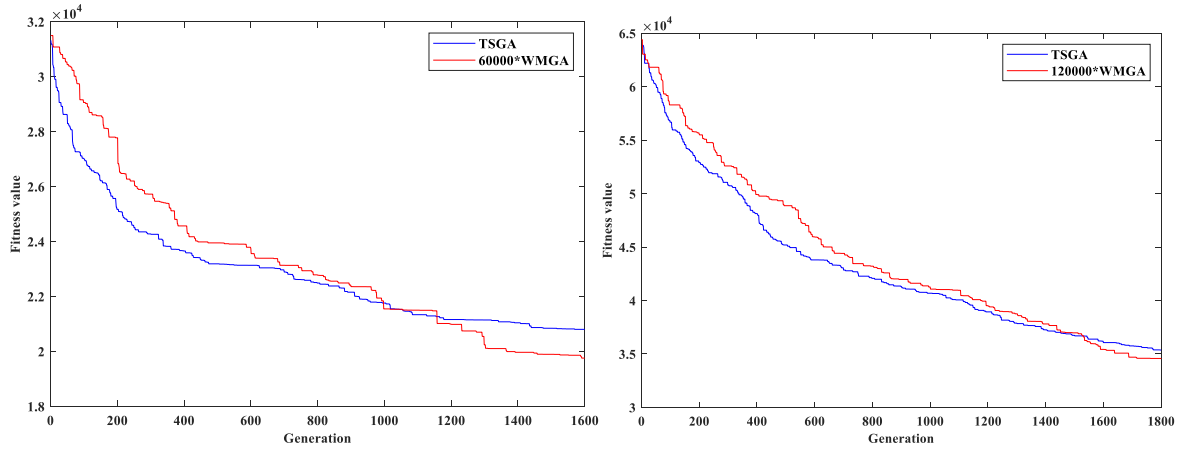

(e) Case 5 (f) Case 6

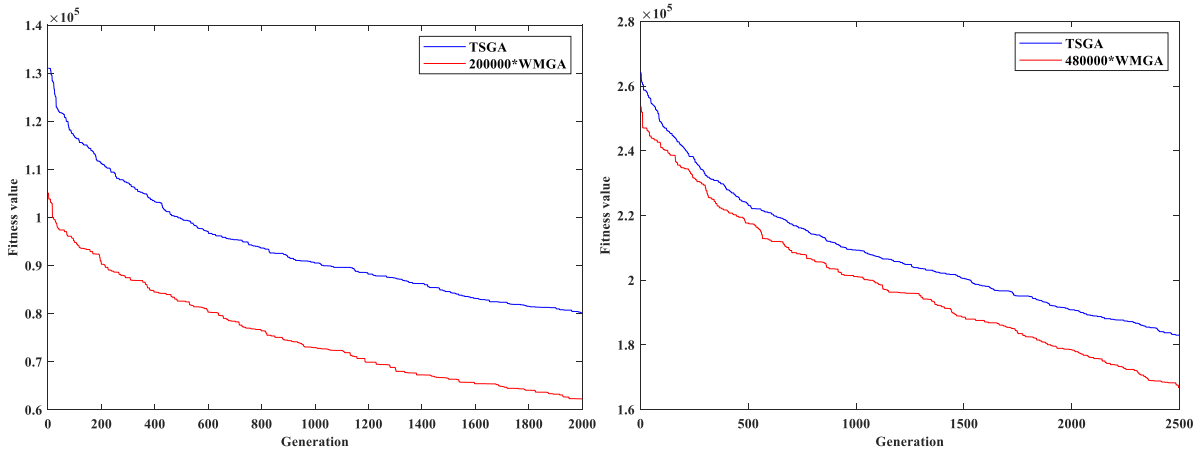

(g) Case 7 (h) Case 8

Fig. 11. Iterations of fitness function values obtained by TSGA and WMGA.

The iterative curves depicting the best fitness values of the populations in each generation of TSGA and WMGA are displayed in Fig. 11. For similar reasons as with the PF diagrams, one diagram out of every four in each case is chosen to be represented. It's worth noting that the fitness values of WMGA are confined within the range of 0 to 1, which is relatively small. If these values were plotted on the same graph as TSGA, it would result in a significant incongruity in the dimensions. To facilitate visual and convenient observation, the best fitness values of WMGA have been magnified by applying a scaling coefficient.

Observing Fig. 11, it becomes evident that in Cases 1-5, the iterative curves either converge or nearly converge. However, in Cases 6-8, the curves exhibit a distinct non-convergent pattern, showing a tendency to decrease. Given more computation time, it is likely that the curves in Cases 6-8 would continue to decline. Nevertheless, such an extension of the computation time of TSGA and WMGA is unnecessary as it would not contribute to a fair comparison, and the current situation more accurately reflects the algorithm's real-world performance. This phenomenon may also shed light on why, in large-scale Cases 6-7, the gaps between DA and the second-ranked methods do not widen further as the case scale increases. This could be attributed to the fact that these methods fail to converge in large-scale scenarios due to limitations in the number of iterative generations. Consequently, their optimal performance in achieving objectives is not fully realized.

TSGA places its primary focus on optimizing *makespan*, which explains its superior performance in small-scale cases with regard to *makespan*. While the robustness of the scheduling plans generated by TSGA may not be as strong as other methods, the deficiencies in robustness can be compensated for by a significantly

improved *makespan*. It's worth noting that when comparing two pre-scheduling plans with similar *makespans*, the one with greater robustness is considered better during execution (Cai et al., 2023a). This rationale underlies the decision to assign the smallest weighted coefficient to robustness when compared to *makespan* and *energy* in this study. However, it's important to recognize that TSGA's advantage in terms of *makespan* diminishes in large-scale cases. Furthermore, the energy consumption indicators for TSGA consistently show no advantage, suggesting that solely focusing on optimizing *makespan* may not be a prudent approach. Additionally, WMGA's performance is even less favorable, highlighting the importance of Pareto-based multi-objective optimization methods.

5.2.3. Gantt chart of the scheduling plans produced by the MoGA-CoD-FCE method

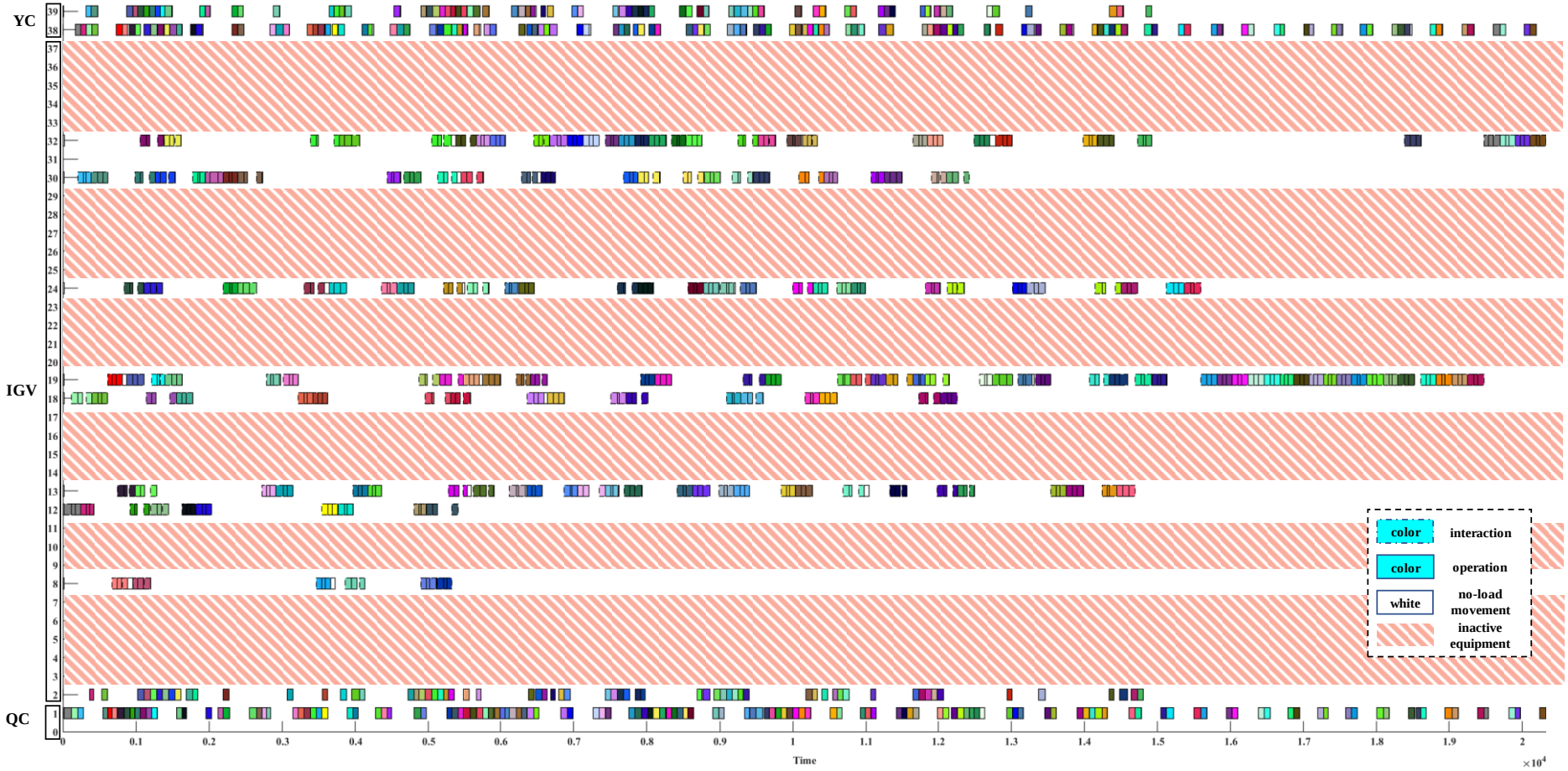

Fig. 12. Scheduling plan generated by the developed MoGA-CoD-FCE in Case 5 under the uncertainty degree of 10-0.08-0.6.

To substantiate the practicality of the pre-scheduling plans generated by the methods under scrutiny, Fig. 12. provides a Gantt chart that illustrates the scheduling plan generated by MoGA-CoD-FCE for Case 5 under the uncertainty conditions of 10-0.08-0.6, encompassing a total of 200 scheduled containers.

The Gantt chart provides insight into the no-load movement time of the equipment and the interaction time between the IGVs and cranes, reflecting a closer alignment with real-world scenarios. During crane loading or unloading operations, the corresponding IGVs are immobilized at the loading or unloading point until the crane completes its task, leading to interaction time. Fig. 12 also reveals a double-cycling operation of IGVs, wherein an IGV swiftly transitions from handling an import container to managing an export container transport task. This serves as evidence affirming the correctness of the developed model and algorithm.

Furthermore, the developed model and algorithm excel at optimizing resource allocation by determining the optimal number of IGVs within a specified maximum limit. As observed in Fig. 12, the cranes are frequently occupied due to their limited quantity, while the abundance of IGVs results in lower utilization rates. Notably, not all IGVs are actively engaged; for instance, IGV 3-7, IGV 9-11, IGV 14-17, IGV 20-23, IGV 25-29, IGV 31, IGV 33-37, etc., remain inactive. Indeed, deploying more IGVs might reduce the *makespan* but could potentially lead to increased *energy consumption*. This phenomenon helps clarify the synchronized trends observed in the *makespan* and *energy consumption* indicators to a certain extent. It underscores that by reducing the number of IGV configurations while concurrently improving IGV utilization, it is possible to lower the *makespan* and enhance IGV utilization, thus leading to a reduction in *energy consumption* simultaneously.

5.2.4. Gantt charts of the scheduling plans with varying levels of robustness

Fig. 13. Two scheduling plans for Case 4, showcasing low and high degrees of robustness.

To further analyze the efficacy of the robustness assessment method AEREI employed in this study, Gantt charts for two distinct scheduling plans in Case 4, with low and high degrees of AEREI, are presented as illustrations in Fig. 13. It is evident that the scheduling plan with lower robustness features fewer time intervals and a more concentrated distribution, with 6 IGVs inactive, whereas the plan with higher robustness displays more time intervals distributed more uniformly. These time intervals can partially absorb the fluctuations in uncertain operation time, with the effect becoming more pronounced at larger case scales. However, it is important to note that the *robustness* index may conflict with the *makespan* and *energy consumption* indices, where higher *robustness* is often associated with poorer *makespan* and *energy efficiency*. This underscores the necessity for employing tri-objective optimization in this study.

5.3. Implications

This research has the potential to bring about substantial enhancements in both operational efficiency and energy efficiency within the context of port operations. Moreover, its incorporation of uncertainty considerations makes it particularly applicable to real-world port environments where operational durations often remain uncertain. In contrast to conventional methods primarily focused on optimizing *makespan*, our developed approach demonstrates significant advantages, especially in larger-scale scenarios involving the scheduling of 2,000 containers. In such cases, our method can yield considerable benefits, including a

reduction in completion time of approximately 9.5 hours and a decrease in energy consumption by about 900 kW·h. In terms of *makespan*, each container can realize an average time savings of about 17 seconds in large-scale optimization. Concerning *energy consumption*, each container can reduce its energy consumption by an average of approximately 0.45 kW·h, as evidenced by our experimental results when compared to traditional methods. By extrapolating from these findings, it is reasonable to assume that for a typical container port handling one million containers annually, potential energy savings of 450,000 kW·h can be achieved, compared to traditional optimization methods that focus solely on *makespan*. Such savings have the potential to significantly benefit the port industry by reducing operational costs and enhancing environmental sustainability.

In terms of the practical application of the developed method, in the largest-scale case involving the handling of 2,000 containers, the computation time on the PC is approximately 7.5 hours after 2,500 iterative generations, which is deemed acceptable. When implemented in an actual port environment, the computational tasks can be offloaded to high-performance cloud computing platforms. This would lead to a significant reduction in computation time as the number of iterative generations, allows for further optimization of the scheduling plan. Furthermore, ports can proactively coordinate with shipping companies to receive task information in advance (H. Li et al., 2023a). This proactive approach empowers the port to execute optimization procedures well in advance, rendering computational times a non-issue (H. Li et al., 2023b).

From a societal perspective, this research holds the potential to deliver multiple benefits. It can not only enhance the efficiency and competitiveness of ports but also bolster the capacity of regions or nations to function as key logistics hubs. Furthermore, it aligns with the global objective of achieving carbon neutrality and contributes significantly to the broader cause of environmental protection, energy conservation, and reducing carbon emissions on a global scale.

Furthermore, given the ubiquity of operation time uncertainty and energy-saving requirements across various scenarios, the proposed framework methodology is versatile and applicable not only in port scheduling, but also in robust, energy-efficient scheduling of multi-equipment systems in manufacturing workshop production, warehousing sorting, and other contexts.

As a result, key implications for stakeholders are systematically summarized in Table 7.

Table 7. Key implications for stakeholders.

Implication	Description	Stakeholders
Operational Efficiency	The research has the potential to substantially enhance operational efficiency in port operations, particularly in larger-scale scenarios, resulting in reduced completion times and improved productivity.	Port Authorities, Port Operators, Shipping Companies
Energy Efficiency	The developed method can lead to significant energy savings in port operations, benefiting both cost reduction and environmental sustainability.	Port Authorities, Port Operators, Environmental Agencies, Energy Providers
Cost Reduction	The reduction in completion time and energy consumption can lead to operational cost savings for ports, potentially amounting to substantial financial benefits.	Port Authorities, Port Operators, Shipping Companies, Investors
Environmental Sustainability	The research aligns with the global goal of achieving carbon neutrality by contributing to reduced carbon emissions and energy conservation in port operations.	Environmental Agencies, Governments, Port Authorities

Logistics Hub Development	Enhancing port efficiency and competitiveness can position regions or nations as key logistics hubs, fostering economic growth and development.	Local Governments, Regional Development Agencies
Versatile Methodology	The proposed framework methodology is versatile and applicable beyond port scheduling, extending to other contexts such as manufacturing workshop production and warehousing sorting for robust, energy-efficient scheduling.	Manufacturing Companies, Warehouse Operators, Logistics Service Providers

6. Conclusion and future work

It is pivotal to ensure port operational and energy efficiency simultaneously to bolster its competitiveness. The task can be pursued through two primary avenues: the adoption of emerging technologies and the optimization of operations. From a technology standpoint, the adoption of a U-shaped port layout and the implementation of a double-cycling operational mode are evident to significantly reduce equipment operational durations and energy consumption, contributing to efficiency gains. On the operational front, the development of suitable mathematical models and solution algorithms is essential for achieving integrated scheduling of port resources, including QCs, IGVs, and YCs. Furthermore, it is critical to address the pervasive issue of uncertainty in operation time within the port environment. This paper addresses these challenges by formulating a new tri-objective optimization problem, encompassing *makespan*, *energy consumption*, and scheduling plan *robustness*, thus providing a comprehensive approach to improving port efficiency and competitiveness.

In this research, the primary focus is placed on the development of a tri-objective mathematical model incorporating the double-cycling operational mode. Furthermore, with regard to the solution algorithm, the necessary chromosome coding, encoding, crossover, and mutation rules have been meticulously designed, all tailored to the problem's unique characteristics. This study brings a significant innovation in port scheduling—a novel dynamic fitness evaluation method selection mechanism that incorporates two operators: the developed crowding distance operator based on an objective value vector cosine distance, and the fuzzy correlation entropy coefficient operator. In the initial phase of the algorithm's iterations, the novel crowding distance operator is primarily employed to enhance population diversity. Conversely, in the later stages, the fuzzy correlation entropy coefficient operator is favored to efficiently select solutions and accelerate convergence. This approach substantially enhances the algorithm's effectiveness without noticeably increasing computation time. The experimental results based on U-shaped port layout cases provide insightful analysis and meaningful implications for the port industry, thereby shedding light on pathways for enhancing operational efficiency and competitiveness.

Nonetheless, it is important to acknowledge the limitations of this paper. For instance, the implementation of the double-cycling operational mode is contingent on the accessibility of container task information, which can pose challenges in certain operational contexts, rendering the problem more complex to address. Some avenues for future research are as follows. The uncertainty can be examined in greater detail, encompassing a wider array of uncertainty types and enhancing the understanding of the predictability of uncertainty. Furthermore, visual simulation software like *AnyLogic* and *Plant Simulation* can be employed to facilitate the creation of an experimental environment that closely emulates an actual port.

Disclosure statement

No potential conflict of interest was reported by the authors.

Acknowledgments

This research was supported by the National Natural Science Foundation of China under Grants 62173263 and 72301203.

References

Ahmed, E., El-Abbasy, M.S., Zayed, T., Alfalah, G., Alkass, S., 2021. Synchronized scheduling model for container terminals using simulated double-cycling strategy. Comput Ind Eng 154, 107118. https://doi.org/10.1016/j.cie.2021.107118

Cahyono, R.T., Kenaka, S.P., Jayawardhana, B., 2022. Simultaneous allocation and scheduling of quay cranes, yard cranes, and trucks in dynamical integrated container terminal operations. IEEE Trans Intell Transp Syst 23, 8564–8578. https://doi.org/10.1109/TITS.2021.3083598

Cai, L., Guo, W., He, L., Li, W., 2023a. Port integrated scheduling under uncertain operation time and cascade effects: A complex network structure entropy solution. Comput. Ind. Eng. 182, 109435. https://doi.org/10.1016/j.cie.2023.109435

Cai, L., Li, W., Luo, Y., 2022. Framework and Algorithm of Customized Workshop Production-logistics Collaborative Scheduling. J Mech Eng 58, 214–226. https://doi.org/10.3901/JME.2022.07.214

Cai, L., Li, W., Luo, Y., He, L., 2023b. Real-time scheduling simulation optimisation of job shop in a production-logistics collaborative environment. Int J Prod Res 61, 1373–1393. https://doi.org/10.1080/00207543.2021.2023777

Cai, L., Li, W., Zhou, B., Li, H., Yang, Z., 2024. Robust multi-equipment scheduling for U-shaped container terminals concerning double-cycling mode and uncertain operation time with cascade effects. Transport Res C-Emer 158, 104447. https://doi.org/10.1016/j.trc.2023.104447

Chargui, K., Zouadi, T., El Fallahi, A., Reghioui, M., Aouam, T., 2021. Berth and quay crane allocation and scheduling with worker performance variability and yard truck deployment in container terminals. Transp Res Pt e-Logist Transp Rev 154, 102449. https://doi.org/10.1016/j.tre.2021.102449

Chargui, K., Zouadi, T., Sreedharan, V.R., Fallahi, A.E., Reghioui, M., 2023. A novel proactive–reactive scheduling approach for the quay crane scheduling problem: a VUCA perspective. IEEE Transactions on Engineering Management 70, 2594–2607. https://doi.org/10.1109/TEM.2022.3151842

Chen, X., He, S., Zhang, Y., Tong, L. (Carol), Shang, P., Zhou, X., 2020. Yard crane and AGV scheduling in automated container terminal: A multi-robot task allocation framework. Transport Res C-Emer 114, 241–271. https://doi.org/10.1016/j.trc.2020.02.012

Dik, G., Kozan, E., 2017. A flexible crane scheduling methodology for container terminals. Flex Serv Manuf J 29, 64–96. https://doi.org/10.1007/s10696-016-9264-4

Guangxi Government, China, 2022. Qinzhou Automated Container Terminal: Pioneering 'Industry-Leading' and Advancing the 'Beibu Gulf Solution.' URL http://bbwb.gxzf.gov.cn/ywdt/t14407748.shtml

Guo, L., Zheng, J., Du, H., Du, J., Zhu, Z., 2022. The berth assignment and allocation problem considering cooperative liner carriers. Transp Res Pt e-Logist Transp Rev 164, 102793. https://doi.org/10.1016/j.tre.2022.102793

Guo, W., Atasoy, B., van Blokland, W.B., Negenborn, R.R., 2021. Global synchromodal transport with dynamic and stochastic shipment matching. Transp Res Pt e-Logist Transp Rev 152, 102404. https://doi.org/10.1016/j.tre.2021.102404

He, J., Huan, Y., Yan, W., Wang, S., 2015. Integrated internal truck, yard crane and quay crane scheduling in

a container terminal considering energy consumption. Expert Syst Appl 42, 2464–2487. https://doi.org/10.1016/j.eswa.2014.11.016
He, J., Tan, C., Zhang, Y., 2019. Yard crane scheduling problem in a container terminal considering risk caused by uncertainty. Adv Eng Inform 39, 14–24. https://doi.org/10.1016/j.aei.2018.11.004
He, L., Chiong, R., Li, W., Dhakal, S., Cao, Y., Zhang, Y., 2022. Multiobjective optimization of energy-efficient job-shop scheduling with dynamic reference point-based fuzzy relative entropy. IEEE T Ind Inform 18, 600–610. https://doi.org/10.1109/TII.2021.3056425
Homayouni, S.M., Tang, S.H., Motlagh, O., 2014. A genetic algorithm for optimization of integrated scheduling of cranes, vehicles, and storage platforms at automated container terminals. Journal of Computational and Applied Mathematics, Fourth International Conference on Finite Element Methods in Engineering and Sciences (FEMTEC 2013) 270, 545–556. https://doi.org/10.1016/j.cam.2013.11.021
Iris, Ç., Lam, J.S.L., 2019. A review of energy efficiency in ports: Operational strategies, technologies and energy management systems. Renewable and Sustainable Energy Reviews 112, 170–182. https://doi.org/10.1016/j.rser.2019.04.069
Ji, B., Yuan, X., Yuan, Y., 2019. A Hybrid Intelligent Approach for Co-Scheduling of Cascaded Locks With Multiple Chambers. IEEE T Cybernetics 49, 1236–1248. https://doi.org/10.1109/TCYB.2018.2799303
Lee, B.K., Low, J.M.W., Kim, K.H., 2015. Comparative evaluation of resource cycle strategies on operating and environmental impact in container terminals. Transportation Research Part D: Transport and Environment 41, 118–135. https://doi.org/10.1016/j.trd.2015.09.014
Li, H., Jiao, H., Yang, Z., 2023a. Ship trajectory prediction based on machine learning and deep learning: A systematic review and methods analysis. Eng Appl Artif Intel 126, 107062. https://doi.org/10.1016/j.engappai.2023.107062
Li, H., Jiao, H., Yang, Z., 2023b. AIS data-driven ship trajectory prediction modelling and analysis based on machine learning and deep learning methods. Transp Res Pt e-Logist Transp Rev 175, 103152. https://doi.org/10.1016/j.tre.2023.103152
Li, H., Yang, Z., 2023. Incorporation of AIS data-based machine learning into unsupervised route planning for maritime autonomous surface ships. Transp Res Pt e-Logist Transp Rev 176, 103171. https://doi.org/10.1016/j.tre.2023.103171
Li, L., Li, Y., Liu, R., Zhou, Y., Pan, E., 2023. A Two-stage Stochastic Programming for AGV scheduling with random tasks and battery swapping in automated container terminals. Transp Res Pt e-Logist Transp Rev 174, 103110. https://doi.org/10.1016/j.tre.2023.103110
Li, W., Cai, L., He, L., Guo, W., 2024. Scheduling techniques for addressing uncertainties in container ports: A systematic literature review. Applied Soft Computing 162, 111820. https://doi.org/10.1016/j.asoc.2024.111820
Li, W., He, L., Cao, Y., 2022. Many-objective evolutionary algorithm with reference point-based fuzzy correlation entropy for energy-efficient job shop scheduling with limited workers. IEEE T Cybernetics 52, 10721–10734. https://doi.org/10.1109/TCYB.2021.3069184
Liu, B., Li, Z.-C., Wang, Y., 2022. A two-stage stochastic programming model for seaport berth and channel planning with uncertainties in ship arrival and handling times. Transp Res Pt e-Logist Transp Rev 167, 102919. https://doi.org/10.1016/j.tre.2022.102919
Lu, Y., Le, M., 2014. The integrated optimization of container terminal scheduling with uncertain factors. Comput Ind Eng 75, 209–216. https://doi.org/10.1016/j.cie.2014.06.018

Niu, Y., Yu, F., Yao, H., Yang, Y., 2022. Multi-equipment coordinated scheduling strategy of U-shaped automated container terminal considering energy consumption. Comput Ind Eng 174, 108804. https://doi.org/10.1016/j.cie.2022.108804

Rodrigues, F., Agra, A., 2022. Berth allocation and quay crane assignment/scheduling problem under uncertainty: A survey. Eur. J. Oper. Res. 303, 501–524. https://doi.org/10.1016/j.ejor.2021.12.040

Stockmann, C., Winkler, H., Kunath, M., 2021. Robustness assessment in production systems. J Manuf Technol Mana 32, 932–951. https://doi.org/10.1108/JMTM-06-2020-0223

Tan, C., He, J., 2021. Integrated proactive and reactive strategies for sustainable berth allocation and quay crane assignment under uncertainty. Ann Oper Res. https://doi.org/10.1007/s10479-020-03891-3

Tan, C., Yan, W., Yue, J., 2021. Quay crane scheduling in automated container terminal for the trade-off between operation efficiency and energy consumption. Adv Eng Inform 48, 101285. https://doi.org/10.1016/j.aei.2021.101285

Tang, G., Qin, M., Zhao, Z., Yu, J., Shen, C., 2020. Performance of peak shaving policies for quay cranes at container terminals with double cycling. Simul Model Pract Th 104, 102129. https://doi.org/10.1016/j.simpat.2020.102129

Venturini, G., Iris, Ç., Kontovas, C.A., Larsen, A., 2017. The multi-port berth allocation problem with speed optimization and emission considerations. Transport Res D-Tr E 54, 142–159. https://doi.org/10.1016/j.trd.2017.05.002

Wang, Y.-J., Li, J., Wang, G.-G., 2023. Fuzzy correlation entropy-based NSGA-II for energy-efficient hybrid flow-shop scheduling problem. Knowledge-Based Systems 277, 110808. https://doi.org/10.1016/j.knosys.2023.110808

Wu, E.N.J.I.E., Zhu, J.I.N., 2023. Integrated Proactive-Reactive Approach and a Hybrid Adaptive Large Neighborhood Search Algorithm for Berth and Quay Crane Scheduling Under Uncertain Combination. J Ind Manag Optim 19, 5612–5640. https://doi.org/10.3934/jimo.2022188

Xiang, X., Liu, C., Miao, L., 2018. Reactive strategy for discrete berth allocation and quay crane assignment problems under uncertainty. Comput Ind Eng 126, 196–216. https://doi.org/10.1016/j.cie.2018.09.033

Xin, J., Negenborn, R.R., Corman, F., Lodewijks, G., 2015. Control of interacting machines in automated container terminals using a sequential planning approach for collision avoidance. Transport Res C-Emer 60, 377–396. https://doi.org/10.1016/j.trc.2015.09.002

Xin, J., Negenborn, R.R., Lodewijks, G., 2014. Energy-aware control for automated container terminals using integrated flow shop scheduling and optimal control. Transport Res C-Emer 44, 214–230. https://doi.org/10.1016/j.trc.2014.03.014

Yu, J., Tang, G., Voß, S., Song, X., 2023. Berth allocation and quay crane assignment considering the adoption of different green technologies. Transp Res Pt e-Logist Transp Rev 176, 103185. https://doi.org/10.1016/j.tre.2023.103185

Yue, L.-J., Fan, H.-M., Fan, H., 2023. Blocks allocation and handling equipment scheduling in automatic container terminals. Transport Res C-Emer 153, 104228. https://doi.org/10.1016/j.trc.2023.104228

Zeng, Q., Diabat, A., Zhang, Q., 2015. A simulation optimization approach for solving the dual-cycling problem in container terminals. Marit Policy Manag 42, 806–826. https://doi.org/10.1080/03088839.2015.1043362

Zeng, Q., Yang, Z., 2009. Integrating simulation and optimization to schedule loading operations in container terminals. Comput Oper Res 36, 1935–1944. https://doi.org/10.1016/j.cor.2008.06.010

Zhang, R., Jin, Z., Ma, Y., Luan, W., 2015. Optimization for two-stage double-cycle operations in container

terminals. Comput Ind Eng 83, 316–326. https://doi.org/10.1016/j.cie.2015.02.007
Zhen, L., Hu, H., Wang, W., Shi, X., Ma, C., 2018. Cranes scheduling in frame bridges based automated container terminals. Transport Res C-Emer 97, 369–384. https://doi.org/10.1016/j.trc.2018.10.019
Zhen, L., Zhuge, D., Wang, S., Wang, K., 2022. Integrated berth and yard space allocation under uncertainty. Transp Res Pt B-Methodol 162, 1–27. https://doi.org/10.1016/j.trb.2022.05.011
Zhu, G.-Y., He, L.-J., Ju, X.-W., Zhang, W.-B., 2018. A fitness assignment strategy based on the grey and entropy parallel analysis and its application to MOEA. Eur. J. Oper. Res. 265, 813–828. https://doi.org/10.1016/j.ejor.2017.08.022
Zhu, S., Tan, Z., Yang, Z., Cai, L., 2022. Quay crane and yard truck dual-cycle scheduling with mixed storage strategy. Adv Eng Inform 54, 101722. https://doi.org/10.1016/j.aei.2022.101722